| AD NUMBER |
| --- |
| AD851947 |
| LIMITATION CHANGES |

TO:

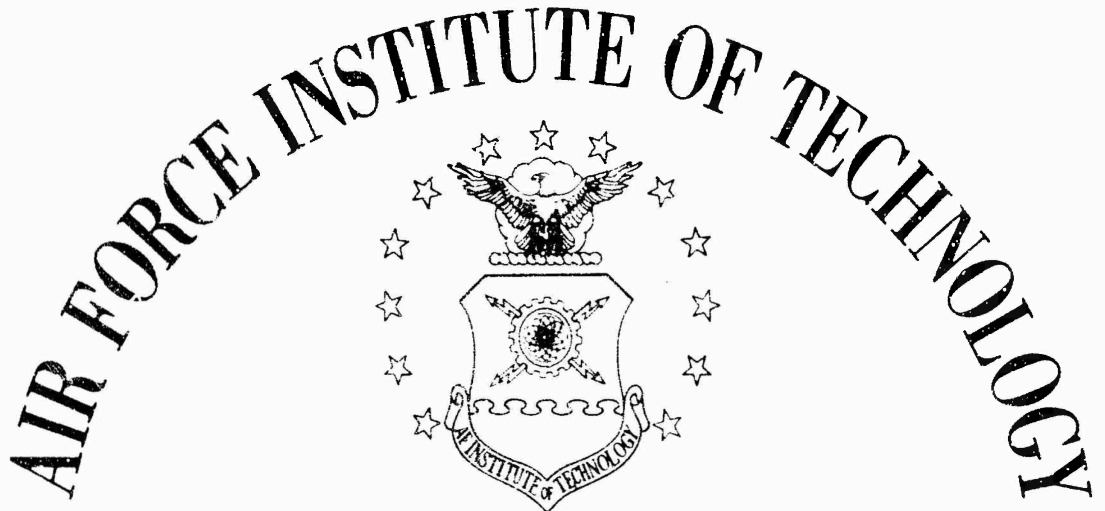Approved for public release; distribution is unlimited.

FROM:

Distribution authorized to U.S. Gov't. agencies and their contractors; Critical Technology; MAR 1969. Other requests shall be referred to Air Force Institute of Technology, School of Engineering, Wright-Patterson AFB, OH 45433. This document contains export-controlled technical data.
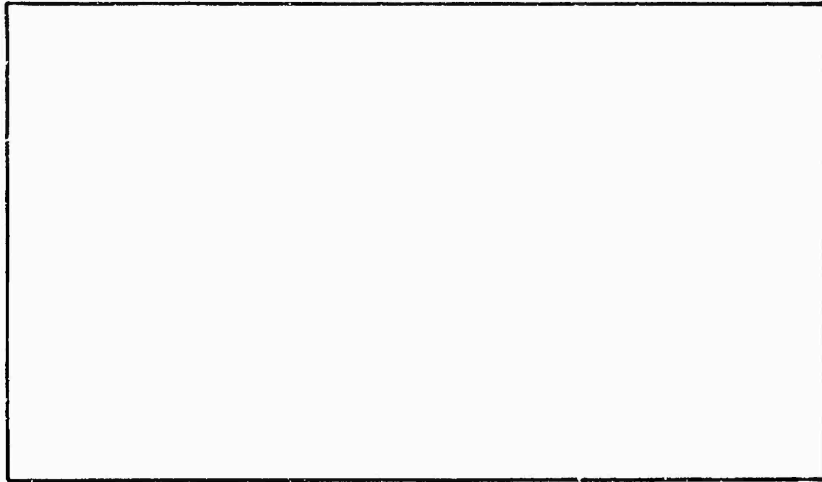
AUTHORITY

AFIT memo, 22 Jul 1971

AD851947

# AIR FORCE INSTITUTE OF TECHNOLOGY

## AIR UNIVERSITY
## UNITED STATES AIR FORCE

# SCHOOL OF ENGINEERING

WRIGHT-PATTERSON AIR FORCE BASE, OHIO

D D C

MAY 1 3 1969

B

AN EXPERIMENTAL STUDY

OF THE EFFECT OF INLET GEOMETRY

ON FLOW AND PERFORMANCE

OF A SUPERSONIC NOZZLE

THESIS

GAM/ME/69-11     Gerald M. Mulenburg
First Lieutenant USAF

AN EXPERIMENTAL STUDY OF THE EFFECT

OF INLET GEOMETRY ON FLOW AND

PERFORMANCE OF A SUPERSONIC NOZZLE


THESIS


Presented to the Faculty of the School of Engineering of

the Air Force Institute of Technology

Air University

in Partial Fulfillment of the

Requirements for the Degree of

Master of Science


by


Gerald M. Mulenburg, B.S.M.E.

First Lieutenant        USAF

Graduate Aerospace-Mechanical Engineering

March 1969

## Preface

In this thesis I have attempted to present the reader with an easily understood report on the evaluation of performance of a two dimensional supersonic nozzle.

I wish to acknowledge my indebtedness to my advisor, Dr. A.J. Shine, Head of the Mechanical Engineering Department, for his valuable advice and patient encouragement throughout the course of this study. I also want to thank my wife for her help in preparation of the many graphs and for typing the complete thesis and my daughter for her exceptionally good behavior during the preparation of this thesis.

## Contents

## List of Figures

## List of Tables

## List of Symbols

| | |
|---|---|
| M | Mach number |
| $M_1$ | Mach number ahead of a normal shock wave |
| $M_2$ | Mach number after a normal shock wave |
| $P_a$ | Barometric pressure |
| $P_o$ | Total (stagnation) pressure |
| $P_{o1}$ | Total pressure ahead of a normal shock wave |
| $P_{o2}$ | Total pressure after a normal shock wave |
| $P_{oc}$ | Total pressure in the calming chamber |
| $P_s$ | Static pressure |
| $\theta$ | Mach angle |
| $\theta'$ | Lip shock angle |

## Abstract

This study is an experimental evaluation of the performance of 12 two-dimensional, converging-diverging, cold flow, supersonic nozzles, each with a different inlet contour but with the same throat and divergent section. The relative efficiency of each nozzle was evaluated by a comparison of total pressure measurements taken in the exit plane, schlieren photographs of the flow, and heat transfer characteristics using moire' patterns. The nozzle with the highest efficiency had an inlet which was an ellipse faired to a $45^{\circ}$ ramp. Its performance was closely followed by that of a nozzle with a circular arc inlet having a radius of three times the throat height. The three nozzles with the lowest efficiencies were those with $30^{\circ}$, $45^{\circ}$, and $60^{\circ}$ linear ramp inlets, respectively. The results of this study indicate that, in nozzle inlet design, a region of immense importance is the curvature just prior to the throat and how this curvature is joined to the throat section.

# I. Introduction

With the extensive use of supersonic nozzles in rockets and aircraft since the end of World War II, much research has been concentrated on improving nozzle performance. Although improvements in nozzle design have increased nozzle efficiency, the resulting nozzles are long and therefore heavy. Reports and experiments (Ref 1,2,5) have suggested that the inlet contour of a supersonic nozzle has a strong influence on the heat transfer in the throat and on the flow in the divergent section. It is theorized that with the proper inlet contour, very short, high expansion, and highly efficient nozzles may be developed.

This thesis was an endeavor to experimentally determine the performance of 12 two-dimensional, converging-diverging, cold flow, supersonic nozzles, each with a different inlet contour but with the same throat and divergent section. The ratio of the inlet length to divergent section length varied from 0.4 to 2.8 for the 12 inlets studied. Determination of the relative efficiency of each nozzle was accomplished by comparison of total pressure measurements taken in the nozzle exit plane, schlieren photographs of the flow, and heat transfer characteristics determined using a moire' optical system (Ref 3).

## II. Apparatus and Procedures

The experimental apparatus consisted of a nozzle body, in which each of the 12 different inlet contours were installed; pressure measuring equipment; and schlieren and moire' flow visualization systems. A brief description of each and its use in the study is given below, and further details with detail drawings may be found in appendix C. A schematic and a photograph of the entire experimental apparatus are shown in fig 6 & 7.

### Nozzle Body and Inlet Contours

The nozzle body and inlet contours were machined from 15/16 in thick plexiglass and mounted in an aluminum frame as shown in fig 1. The nozzle body was designed using one-dimensional isentropic relations (Ref 4) for a pressure ratio of $P_a/P_O = 0.156$ ($M = 1.87$) with an area correction of 5% at the exit for the boundary layer. With a throat height of 0.5 in and an exit opening of 0.8 in, the 15/16 in thick nozzle walls minimized the corner and side wall effects to create a good two dimensional flow.
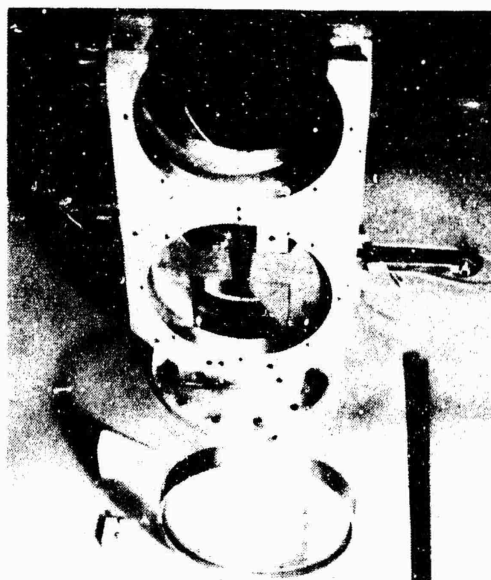


Fig 1 Photograph of Test Section

2

The removeable glass windows permitted schlieren and moire'
photographs to be taken of the flow and also provided access
for changing the inlet sections.

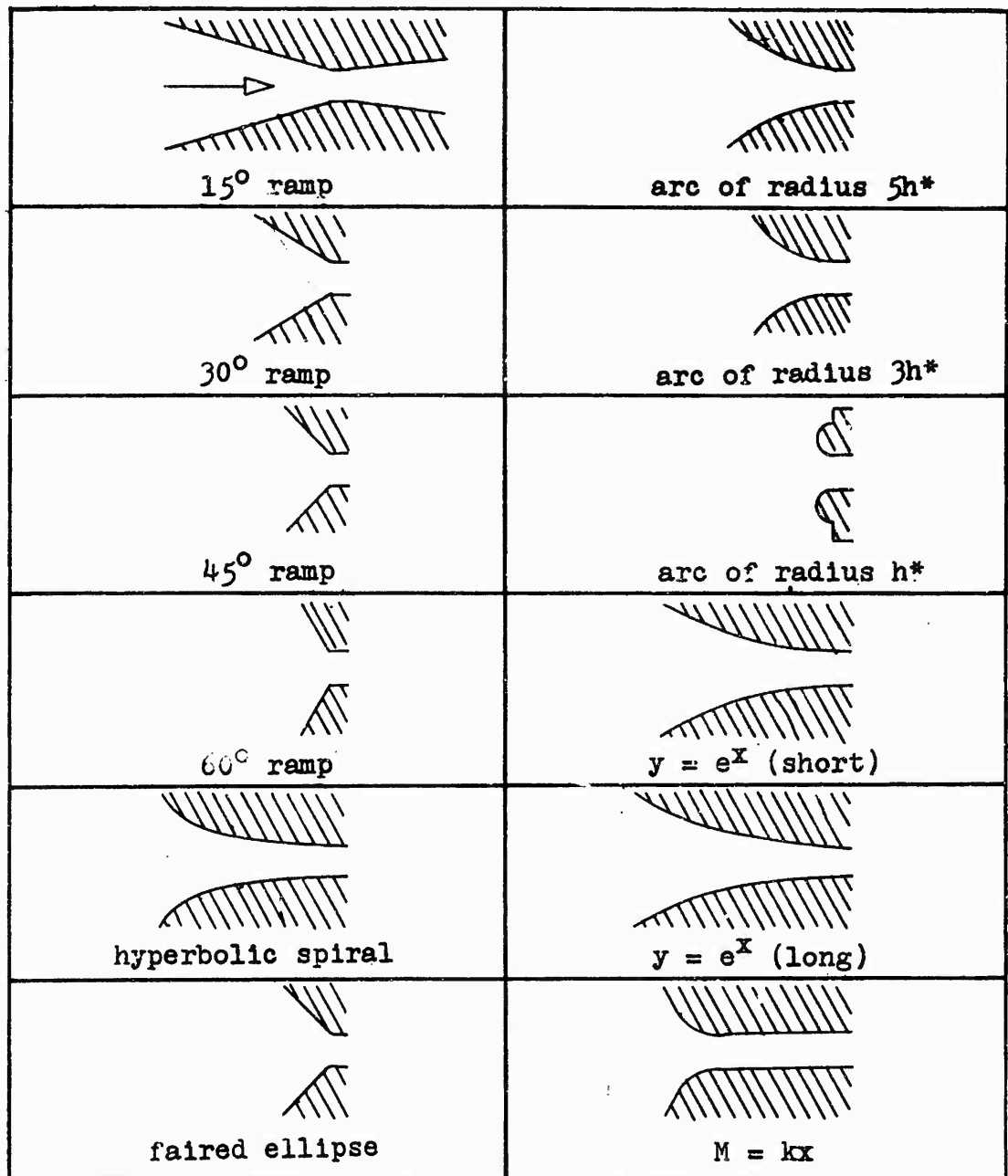The 12 different inlet contours used in the study are
shown in fig 2.

| | |
|---|---|
| 15° ramp | arc of radius 5h* |
| 30° ramp | arc of radius 3h* |
| 45° ramp | arc of radius h* |
| 60° ramp | $y = e^X$ (short) |
| hyperbolic spiral | $y = e^X$ (long) |
| faired ellipse | M = kx |

Fig 2   Nozzle Inlet Contours

## Pressure Measuring Equipment

The traverse mechanism, shown in fig 3, is a simple crank and screw apparatus used to position the pressure sensing hole of either the total or static pressure probe. An indicator on a graduated scale shows the
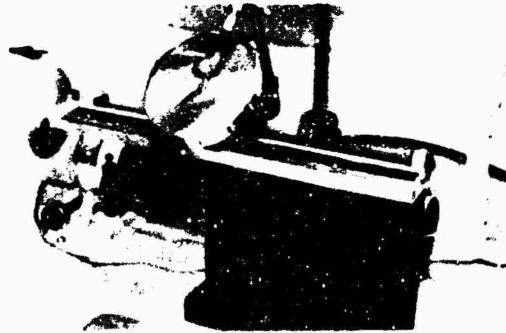


rig 3    Traverse Mechanism

position of the hole relative to some point in the nozzle.

The total pressure probe shown in fig 4, is a 0.036-in-diameter stainless steel tube with a 0.013-in-diameter hole to sense the total pressure in the exit plane. Attached on either side of the pressure sensing hole are two brass bars which slide in teflon guide blocks as shown in fig 5.

The brass bars prevent the tube from twisting thus keeping the pressure sensing hole always facing into the flow. The teflon guide blocks are slotted to allow
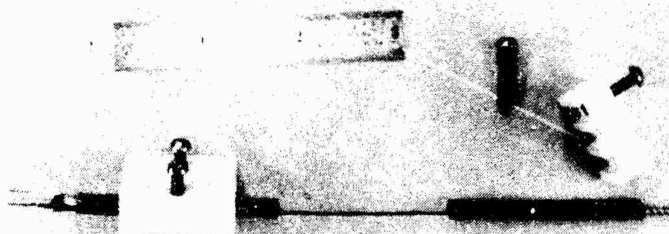


Fig 4    Total Pressure Probe

the probe to be placed in three different transverse positions in the exit plane. One transverse position is on the nozzle centerline with the other two located 9/32 in on either side of the centerline. With the traversing mechanism the pressure sensing hole was moved across the nozzle exit plane.
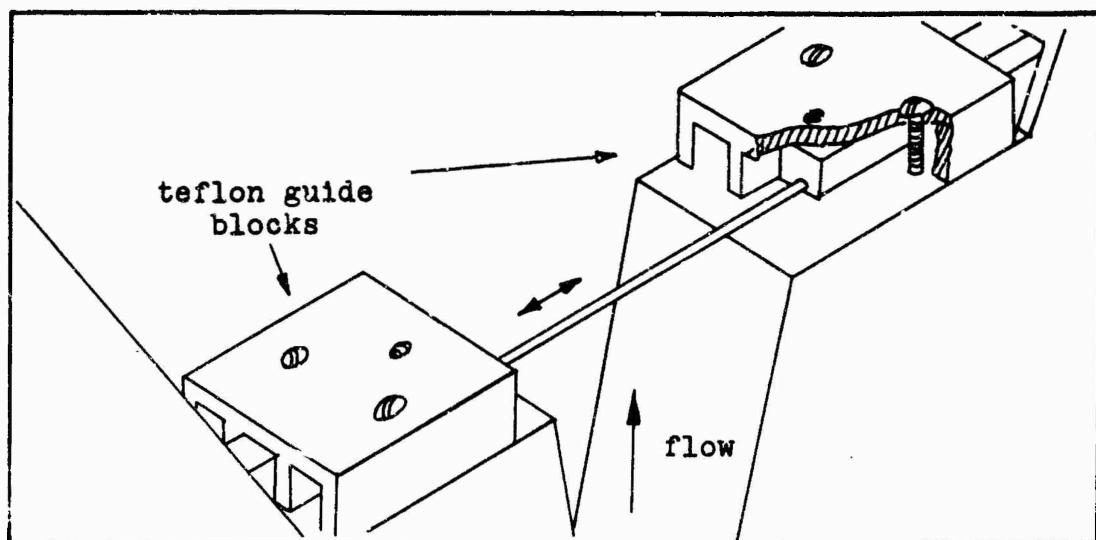
4

Fig 5    Installation of Total Pressure Probe

The static pressure probe is a 0.040-in-diameter stain-less steel tube with a 0.013-in-diameter pressure sensing hole. The probe was positioned along the nozzle axis as shown in fig 6. Two metal guides kept it centered on the nozzle axis at all times and the pressure sensing hole could be positioned anywhere along the axis using the traversing mechanism.

A schematic and photograph of the complete pressure measuring system are shown in figs 6 & 7.


Flow Visualization Systems

A schlieren optical system, fig 8, was used to obtain photographs of the flow at various pressure ratios with a Polaroid camera using ASA 3000 film and 0.5 millisecond spark lamp.

Schematic of Experimental Equipment

Fig 6
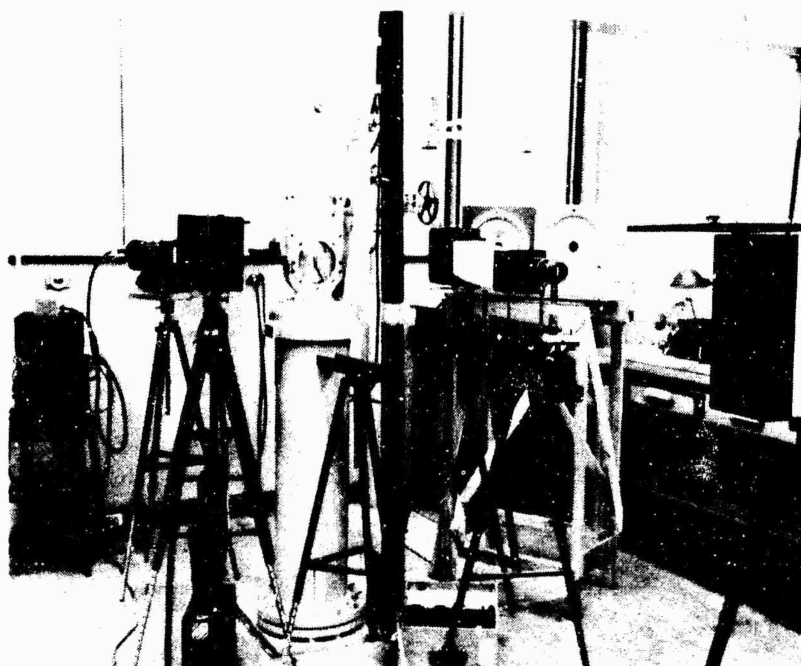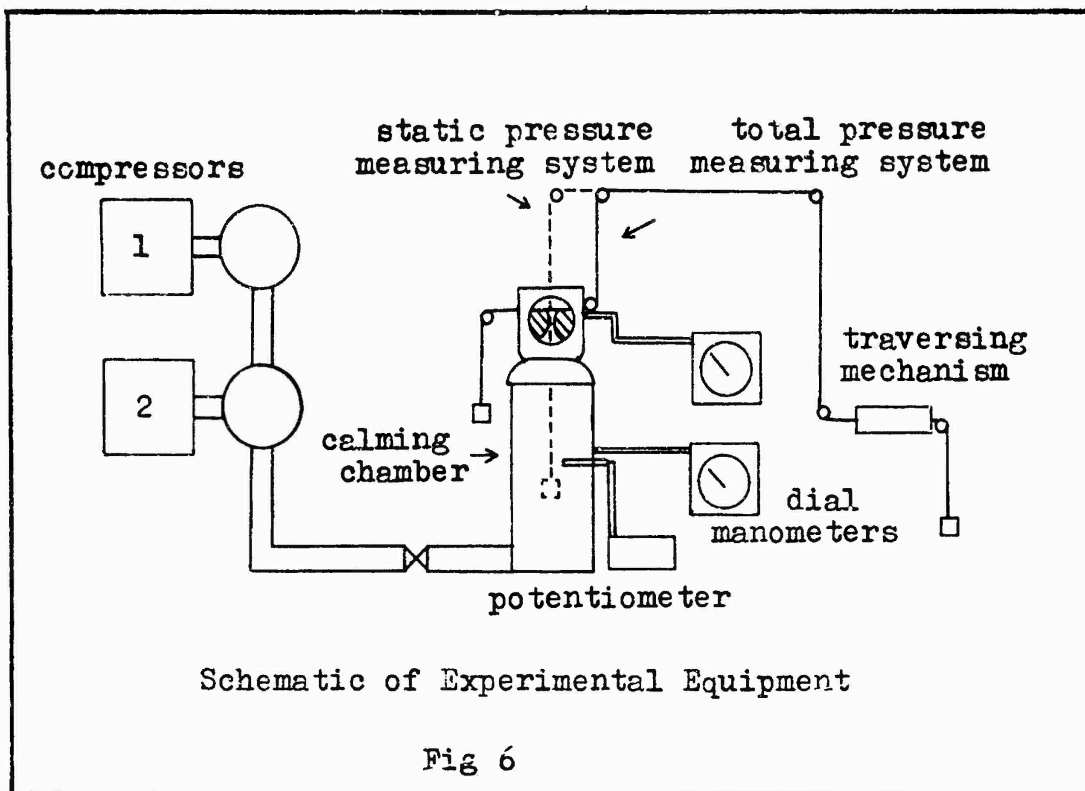


Fig 7    Experimental Apparatus and Equipment

A typical schlieren photo-
graph of the flow is shown
in fig 9 and additional
photographs of each nozzle,
taken at six different
pressure ratios, are
included in appendix A.



parabolic mirror
spark lamp
test section →
camera
knife edge
parabolic mirror

Schlieren Optical System

Fig 8

The moire' optical
system was set up by in-
stalling two, 200 line per
in, diffraction gratings
in the schlieren parallel
light path and removing
the knife edge. A zirconium light source with a yellow
filter was used in conjunction with a Polaroid camera and
ASA 200 film at a 1/40 sec shutter speed to obtain photo-
graphs of the moire' patterns. A typical moire' pattern is
shown in fig 10 and one for each nozzle at the design
pressure ratio $(P_a/P_{oc} = 0.156)$ may be found in appendix A.
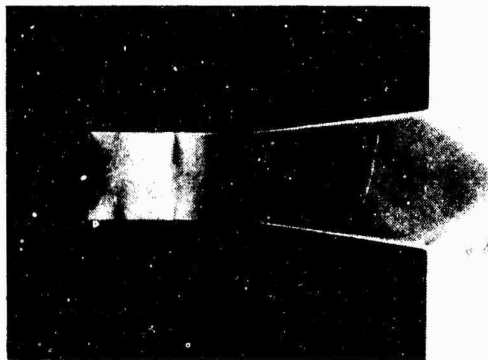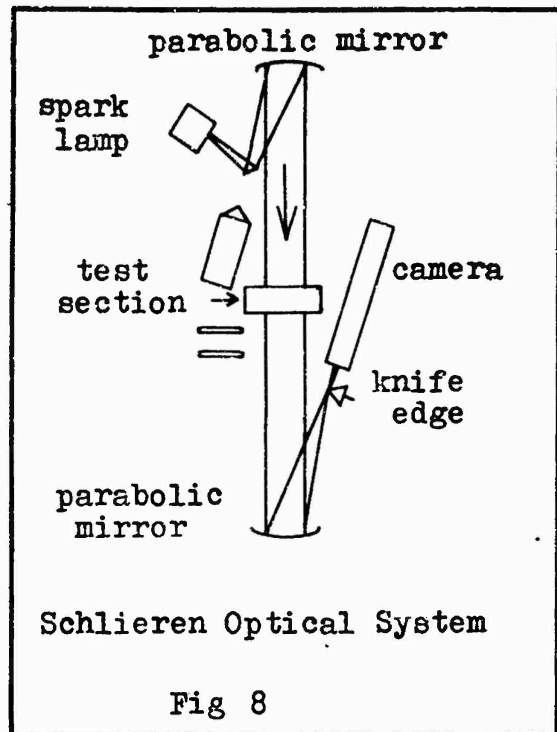


Fig 9    Typical Schlieren
Photograph of the Flow



Fig 10    Typical Moire'
Pattern

## III. Results and Discussion

Typical graphs of the pressure data are shown in fig 11. Graphs of all the pressure measurements may be found in appendix B. In addition, the static and total pressures were non-dimensionalized by dividing by the chamber total pressure $P_{oc}$. These non-dimensional values were then plotted versus distance along the nozzle axis and distance across the nozzle exit, respectively. Fig 12 and 13 are graphs of the nozzles with the highest and lowest efficiency superimposed on the data of the other nozzles to allow a comparison. The sharp dip in the curve of the least efficient nozzle is due to the presence of shock waves.

## Comparison of Total Pressure Measurements

As shown in fig 14, a shock wave was present in front of the total pressure probe. The shock wave was located in, or very nearly in, the exit plane for each operation due to a slight raising of the probe by the momentum of the flow. To correct the pressure readings for the presence of the shock wave, the readings were assumed to have been taken downstream of a normal shock. (The small size of the pressure sensing hole supports this assumption.)

For each nozzle 17 total pressure readings were taken across the exit plane (0.05 in apart) at each transverse position of the probe as shown in fig 15.
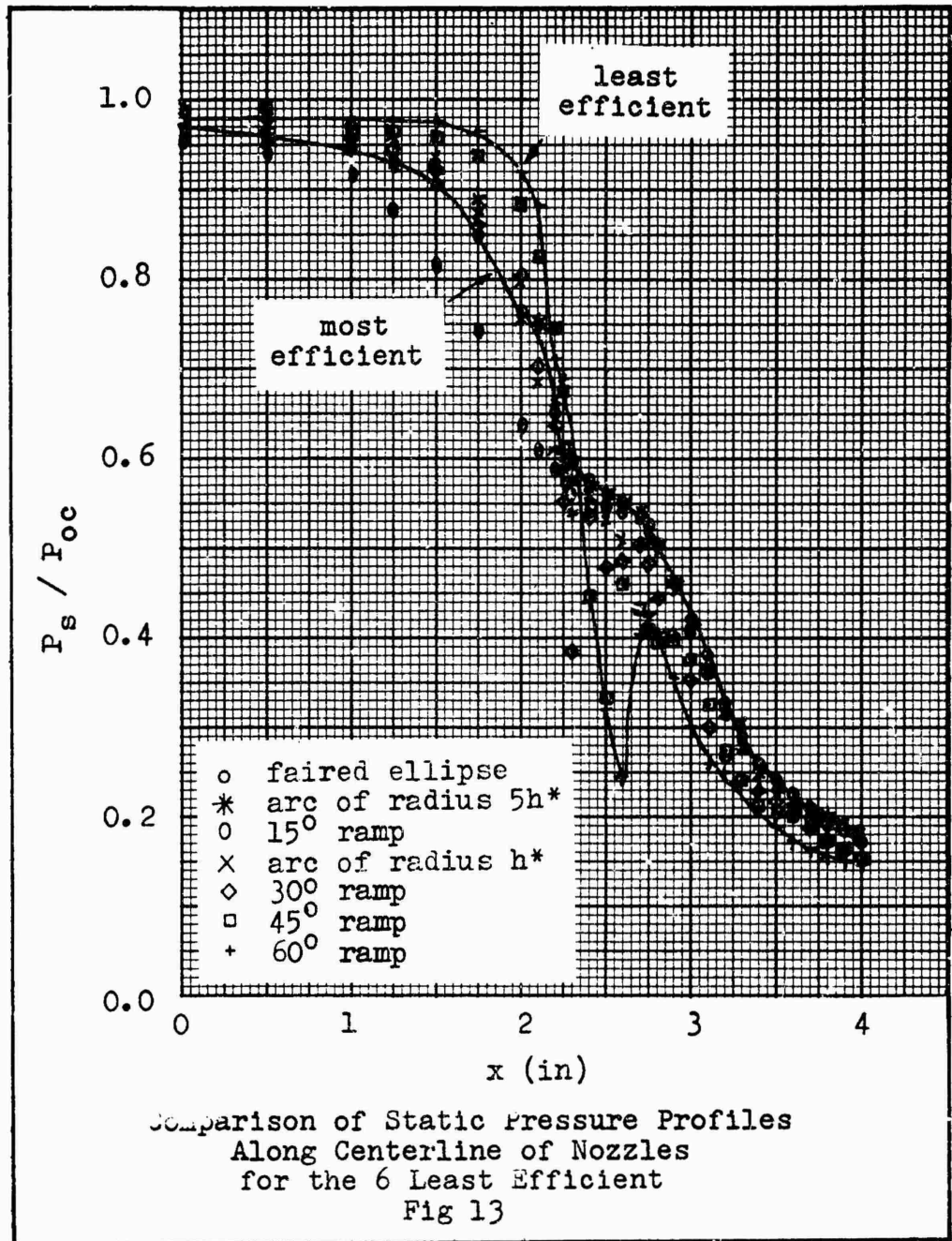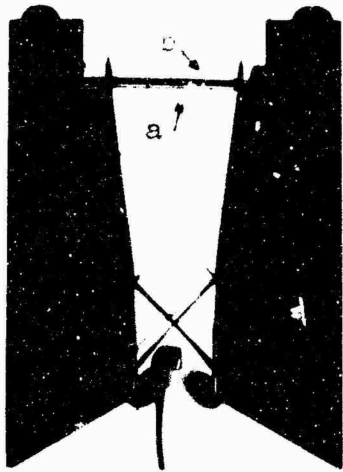
8

Fig 11  Graphs of Experimental Data

Comparison of Static Pressure Profiles
Along Centerline of Nozzles
for the 6 Most Efficient
Fig 12

Comparison of Static Pressure Profiles
Along Centerline of Nozzles
for the 6 Least Efficient
Fig 13
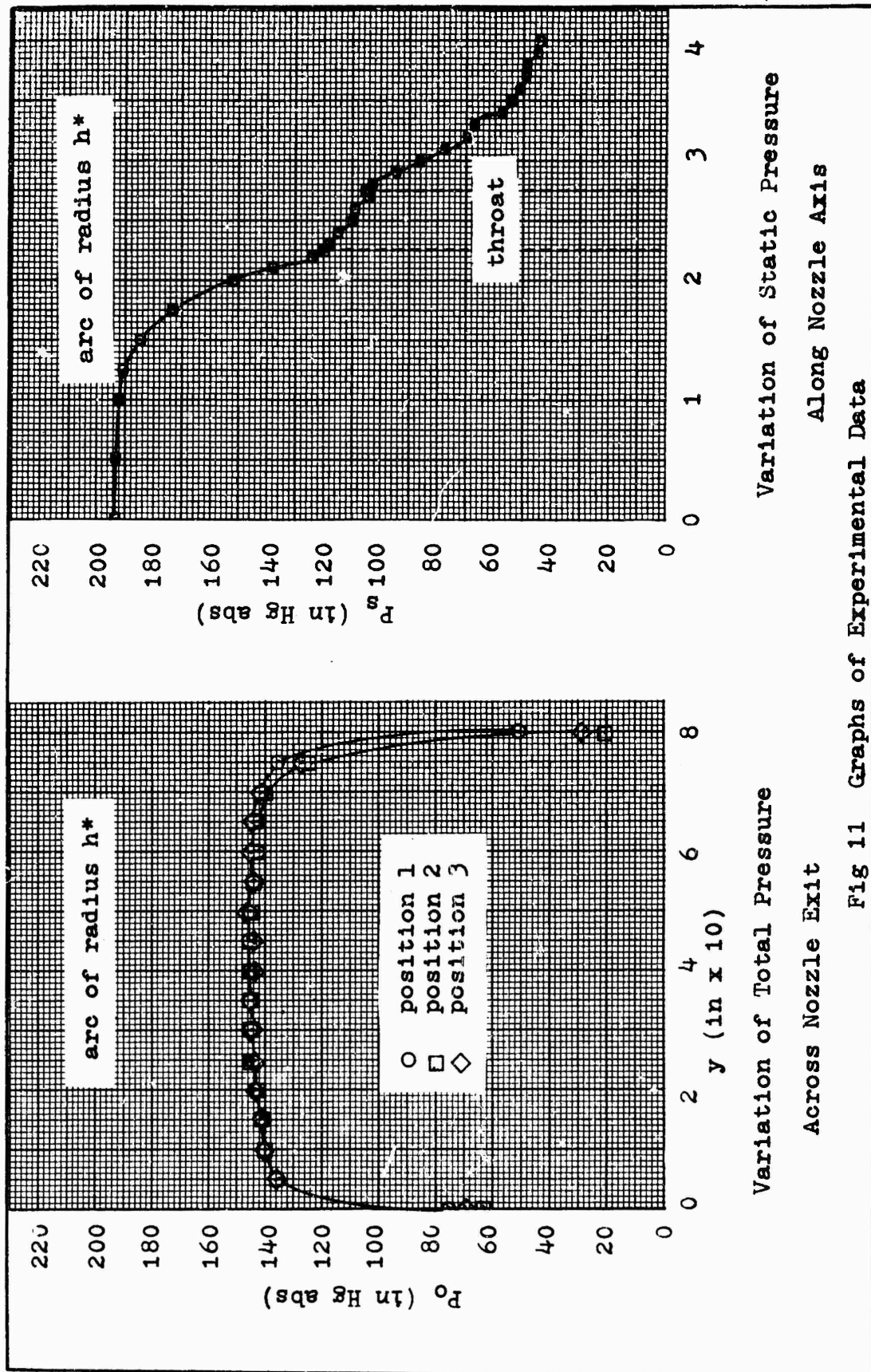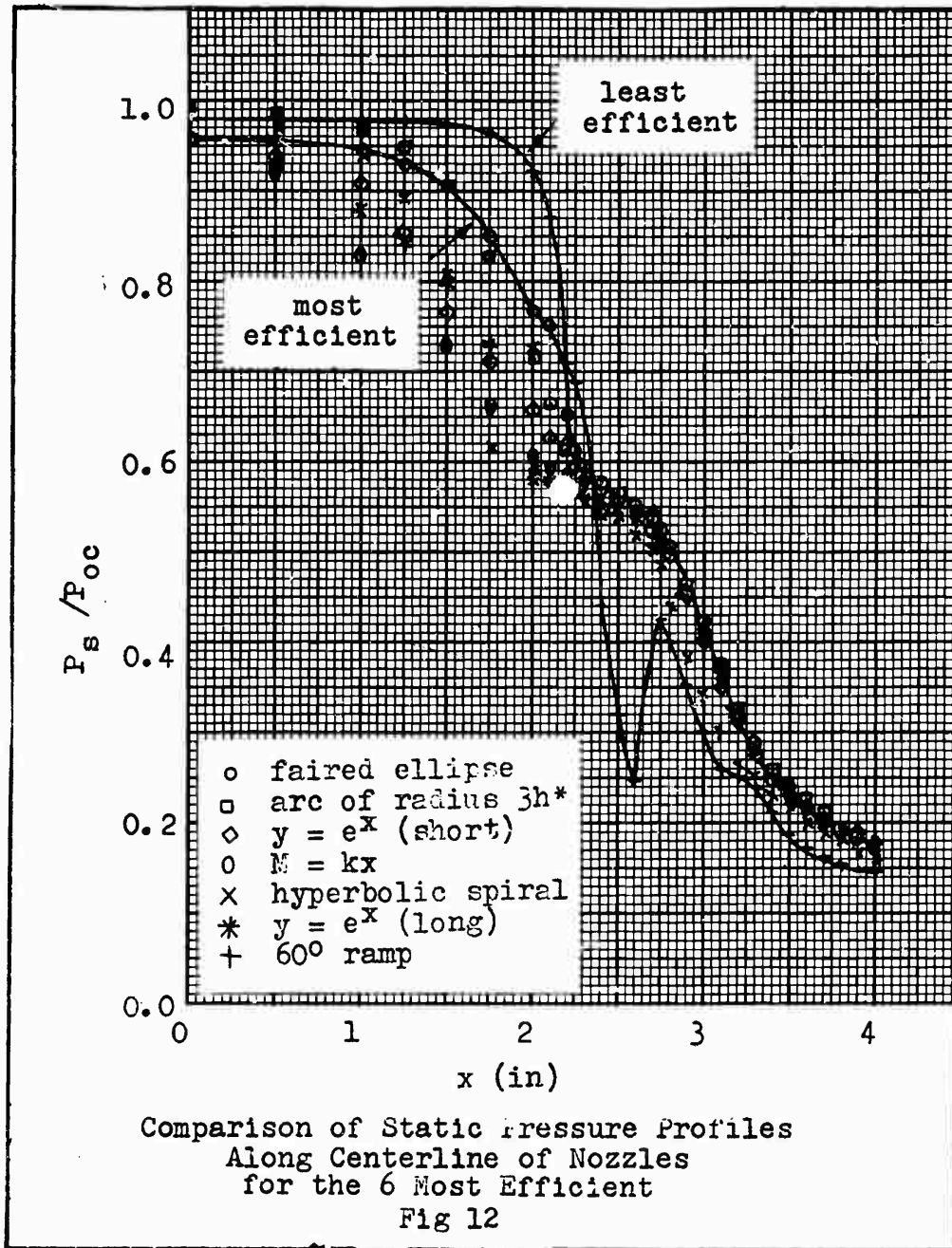
Fig 14    Shadowgraph Showing
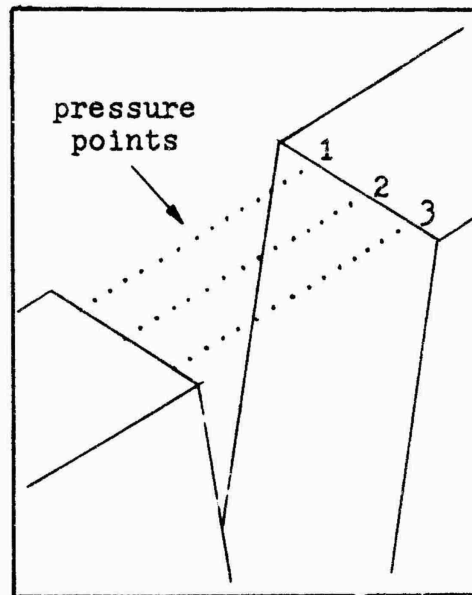Shock Wave in Front of the        Fig 15    Nozzle Exit Plane
Probe    a)Shock Wave b)Probe

An arithmetic average of the readings for each nozzle was cal-
culated excluding the first and last two readings for all
three transverse positions of the probe.  The excluded read-
ings were obtained near the wall'of the nozzle and their
integrity is doubtful since the pressure sensing hole may have
been partially blocked by the wall.  By measuring the angle of
the Mach lines at the exit plane on the schlieren photographs,
it was possible to determine the centerline Mach number using
$M = 1/\sin \theta$.  Two readings of $\theta$ were taken (one each from a
left and right wave) and averaged to obtain the exit Mach
number for each nozzle.  The values of M obtained varied from
a low of 1.75 to a high of 1.96 or approximently $\pm$ 6% of
$M_{design}$.  The angle $\theta$ had a strong effect on the value of the
Mach number and was difficult to measure accurately.

12

Therefore, an arithmetic average of the Mach numbers obtained from all of the photographs was used to correct for the $P_o$ drop across the shock wave in front of the probe. This average Mach number, $M_{avg} = 1.85$, was 0.02 less than the design Mach number, $M_{design} = 1.87$. $M_{avg}$ and the average measured total pressure for each nozzle were then used to determine the total pressure $P_{o1}$ in front of the shock wave using the Gas Tables (Ref4).

Because of the inaccuracies inherent in the calculation of the exit Mach number, the relative values of $P_o$ upstream and downstream of the shock were compared to observe any possible inconsistancies between them. The $P_o$ values were first non-dimensionalized by dividing each by the atmospheric pressure. This permitted more accurate comparison because the tests were conducted at $P_{oc}$ values such that $P_a/P_o = 0.156$. A comparison of the two sets of values is presented in Table I and it is seen that the two sets of values agree with each other. Three significant figures were maintained throughout but a fourth significant figure had to be used to determine the order of the nozzles with regard to efficiency. The efficiencies of the first three nozzles were much closer to each other than that of the last three; this comparison is also shown by a graph of these six in fig 16.

Comparison of the Three Most Efficient
With the Three Least Efficient
Nozzles
Fig 16
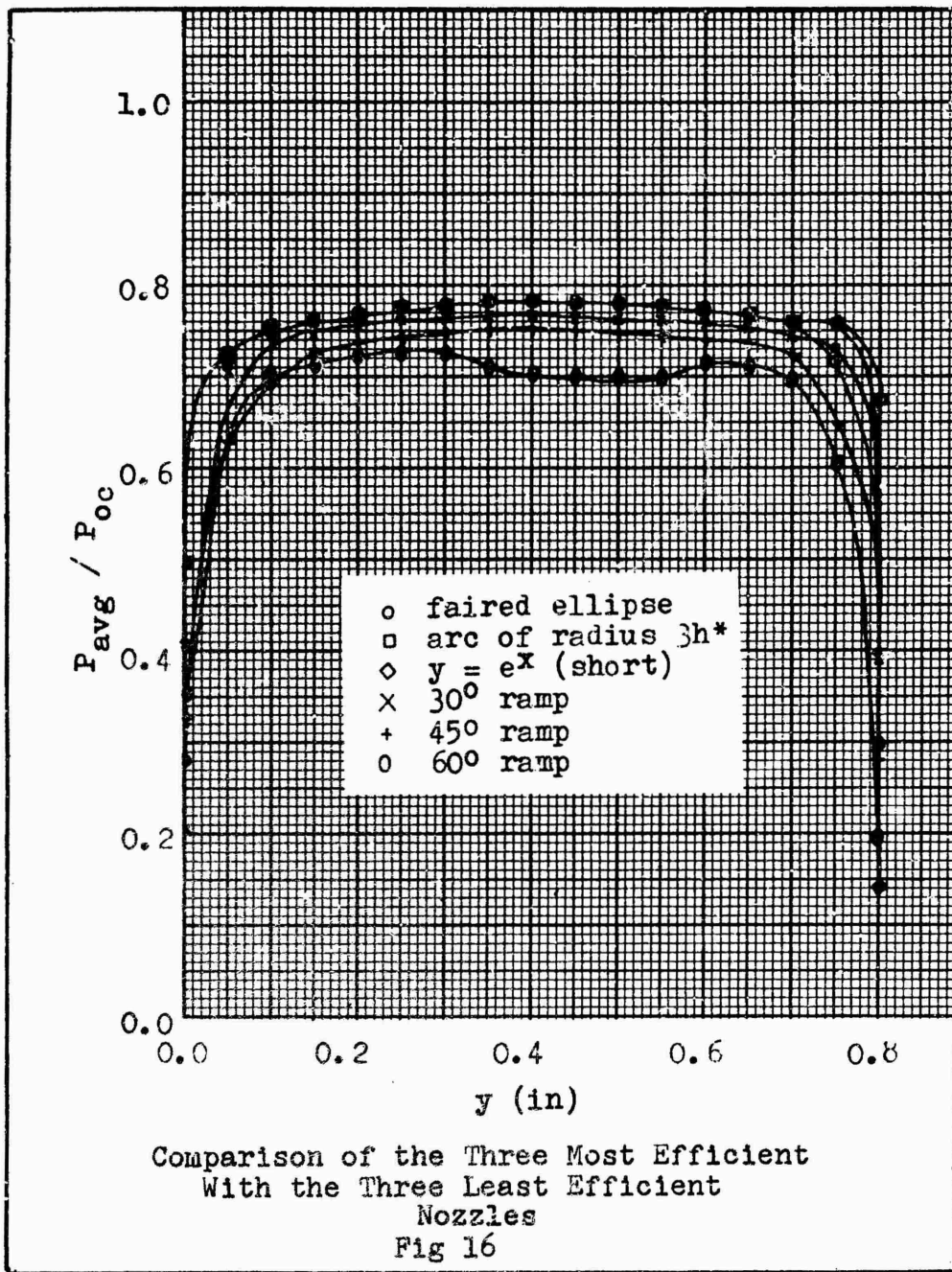
Table I    Performance Ratings Based on Total Pressure

| Inlet | $P_{o2}/P_a$ | $P_{o1}/P_a$ |
|---|---|---|
| (1) faired ellipse | 4.94 | 6.19 |
| (2) arc of radius 3h* | 4.93 | 6.18 |
| (3) $y = e^x$ (short) | 4.92 | 6.17 |
| (4) $M = kx$ | 4.92 | 6.17 |
| (5) hyperbolic spiral | 4.92 | 6.17 |
| (6) $y = e^x$ (long) | 4.92 | 6.17 |
| (7) arc of radius 5h* | 4.92 | 6.17 |
| (8) $15^\circ$ ramp | 4.91 | 6.16 |
| (9) arc of radius h* | 4.90 | 6.14 |
| (10) $30^\circ$ ramp | 4.84 | 6.07 |
| (11) $45^\circ$ ramp | 4.71 | 5.91 |
| (12) $60^\circ$ ramp | 4.54 | 5.69 |

Examination of the Schlieren Photographs

Performance comparisons for the twelve different nozzles using the schlieren photographs were more difficult to determine than from the pressure measurements because the flow patterns in some of the nozzles were quite similar. The number and strength of the shock waves present in the nozzle were used as determining factors of performance in those configurations which had shock waves. The larger the visible density gradient through a shock wave, the lower the performance rating that was assigned to a given nozzle.

15

The interaction of the shock waves with the boundary layer created turbulence along the nozzle wall and this phenomenon (or lack of it) was also used, in addition to the shock waves, as a performance criterion. The Mach angle $\theta$ and the lip shock angle $\theta'$ were also used to estimate performance of the various nozzles, the larger the angle the lower the Mach number and therefore the lower the efficiency. The performance ratings using the above criterion are presented in Table II. The relative efficiency of each nozzle is not identical using each of the above methods of extimating performance, except in a few instances, as is readily noted in the table. This is due to, as mentioned earlier, the difficulty of determining performance because of similarity of some of the flow patterns as well as difficulty in accurately measuring $\theta$ and $\theta'$ from the photographs.

The most interesting result of the schlieren photography was the apparent contact surface evident in the photographs of the nozzle with the inlet having an arc of radius h* as shown in fig 17. The contact surface implies that the main stream of the flow is separated from the nozzle wall by a cooler, more dense layer of air.



Fig 17    Photograph of the Contact Surface

16

Table II    Other Methods of Rating Nozzle Performance

| Inlet | Shocks | $Q$ | $Q'$ |
|---|---|---|---|
| arc of radius 3h* | 1 | 10 | 8 |
| $y = e^x$ (short) | 2 | 3 | 7 |
| $M = kx$ | 3 | 6 | 3 |
| hyperbolic spiral | 4 | 8 | 5 |
| $y = e^x$ (long) | 5 | 5 | 9 |
| arc of radius 5h* | 6 | 1 | 2 |
| faired ellipse | 7 | 4 | 1 |
| arc of radius h* | 8 | 7 | 6 |
| $15^o$ ramp | 9 | 2 | 4 |
| $30^o$ ramp | 10 | 9 | 10 |
| $45^o$ ramp | 11 | 11 | 11 |
| $60^o$ ramp | 12 | 12 | 12 |

## Examination of the Moire' Patterns

The analysis of the moire' patterns was performed by Jones (Ref 3) and only the applicable results will be presented here. Heat transfer is most critical in the nozzle throat, and the method used to rate the various nozzles was to measure the density gradient at the nozzle wall in the throat from the moire' patterns. The density gradients were then used with values of measured static pressure, to calculate the corresponding temperature gradients. The nozzle with the smallest temperature gradient was rated as best.

17

The order of the inlets rated by this method was then com-
pared to the order obtained using the total pressure measur-
ments;  the results are presented in Table III.

Table III    Performance Ratings Based on Exit Total
Pressure and Throat Temperature Gradient

| Inlet | $P_{o2}/P_a$ | $P_{o1}/P_a$ | Throat dT/dy |
|---|---|---|---|
| faired ellipse | 4.94 | 6.19 | 380 |
| arc of radius 3h* | 4.93 | 6.18 | 500 |
| $y = e^x$ (short) | 4.92 | 6.17 | 540 |
| $M = kx$ | 4.92 | 6.17 | 660 |
| hyperbolic spiral | 4.92 | 6.17 | 560 |
| $y = e^x$ (long) | 4.92 | 6.17 | 560 |
| arc of radius 5h* | 4.92 | 6.17 | 740 |
| $15^o$ ramp | 4.91 | 6.16 | 560 |
| arc of radius h* | 4.90 | 6.14 | 720 |
| $30^o$ ramp | 4.84 | 6.07 | 880 |
| $45^o$ ramp | 4.71 | 5.91 | 1500 |
| $60^o$ ramp | 4.54 | 5.69 | 1660 |

In all three columns the three least efficient nozzles
and the three most efficient nozzles are the same and in the
same relative order.  This is extremely encouraging since
using the moire' patterns to determine performance was en-
tirely independent of using the total pressure measurements.

## IV. Conclusions and Recommendations

From the results of this study the following conclusions may be drawn:

1. Of the 12 nozzle inlets tested the $45^{\circ}$ ramp faired to the throat with an ellipse was the most efficient. It resulted in a total pressure loss of 5.85 in Hg while the least efficient inlet, a $60^{\circ}$ ramp, resulted in a 14.5 in Hg loss. The average $P_0$ loss for all the inlets was 9.0 in Hg.

2. Matching the curvature of the inlet to the throat geometry is of extreme importance as can be noted by a comparison of the results of the nozzle with the $45^{\circ}$ ramp inlet (11), to that of the nozzle with a $45^{\circ}$ ramp faired to an ellipse (1).

3. Several of the nozzle inlet designs tested have nearly the same efficiency. This is due to trade-offs between the losses created by differences in the inlet lengths and the losses due to changing the direction of the flow more rapidly.

4. The design of a nozzle inlet with high efficiency requires extreme care to insure smooth turning of the flow.

5. Determination of relative nozzle efficiency using heat transfer rates obtained from moire' patterns is in good agreement with that obtained by measuring the total pressure losses in the nozzle. This is significant because the use of moire' patterns does not disturb the flow as probes do.

6. By proper design of the nozzle inlet a contact surface can be generated which may prove to aid in inlet design.

19

This would be accomplished by creating a layer of cooler, more dense air next to the nozzle wall thereby insulating the nozzle throat from hot gases in the mainstream of the flow.

The recommendations arising out of the course of this study are:

1. Further study of the nozzles with inlets which had high efficiency and variations of these inlets, should be performed to examine the effect of changing parameters such as the inlet to divergent section lengths. Also the maximum possible expansion for a given inlet could be determined by varying the divergence angle and observing separation phenomena.

2. Determination of heat transfer rates by more accurate methods than using moire' patterns is recommended. One method is currently available which consists of applying very thin platinum heat transfer gages to a thin piece of pyrex glass which is formed to take the shape of the nozzle.

3. Additional study of a nozzle with inlets similar to the one with an arc of radius h*, using an interferometer to determine if a strong contact surface exists and how it is produced, could prove to be very important in future nozzle design.

# Bibliography

1. Boldman, D.R., et al. "Effect of Uncooled Inlet Length and Nozzle Convergence Angle on the Turbulent Boundary Layer and Heat Transfer in Conical Nozzles Operating With Air." Journal of Heat Transfer,89:Series B 341-350 (November 1967).

2. Gogish. L.V. "Investigation of Short Supersonic Nozzles." Foreign Technology Division, Translation FTD-HT-23-1079-67, Wright-Patterson Air Force Base, Ohio: Air Force Systems Command, 1 August 1967.

3. Jones, J.T. "Quantitative Gas Flow Measurements Using a Moire' Optical System". Unpublished thesis. Wright-Patterson Air Force Base, Ohio: Air Force Institute of Technology, March 1969.

4. Keenan, J.H. and Kaye, J. Gas Tables. New York: John Wiley and Sons, Inc.,1948.

5. Shapiro, A.H. The Dynamics and Thermodynamics of Compressible Fluid Flow, Vol 1&2. New York: The Ronald Press, 1953.

6. Talmor, E. "Effect of Pressure Gradient on Sonic-Point Heat Transfer." AIChE Journal, 14.1: 127-134, (January 1968).

Appendix A

Photographs of Flow Patterns

(1) faired ellipse
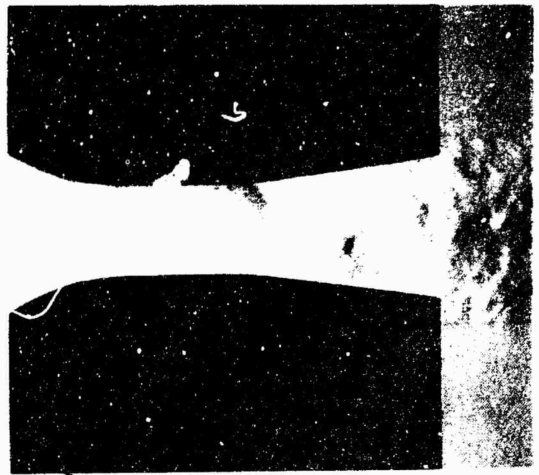
(2) arc of radius 3h*
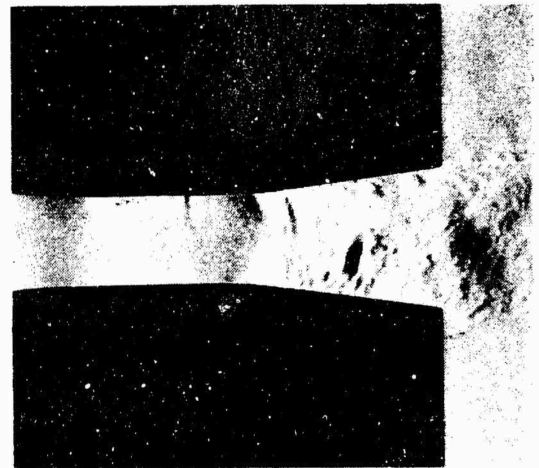
(3) $y = e^x$ (short)

(4) $M = kx$

(5) hyperbolic spiral

(6) $y = e^x$ (long)

Schlieren Pictures of Various Nozzles at $P_a/P_o = 0.667$

Fig A-1

(7) arc of radius 5h*
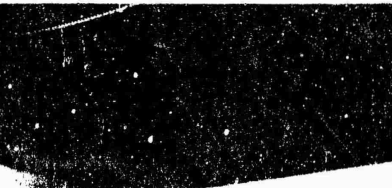
(8)     15° ramp
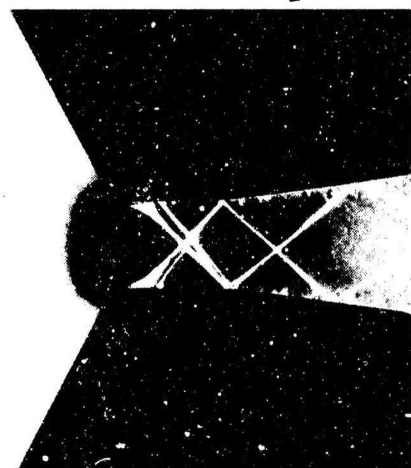
(9) arc of radius h*

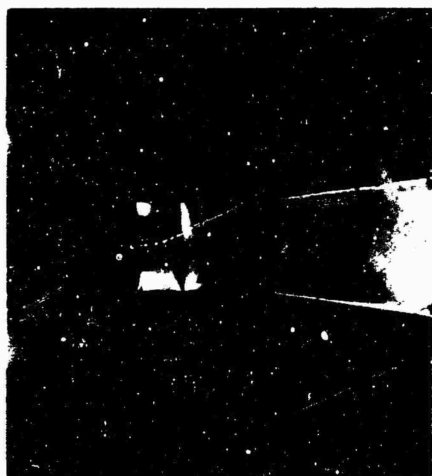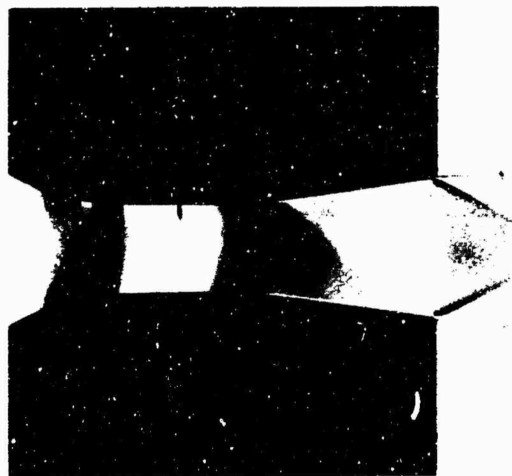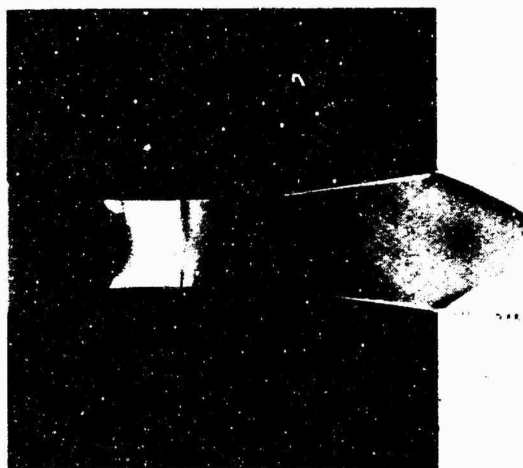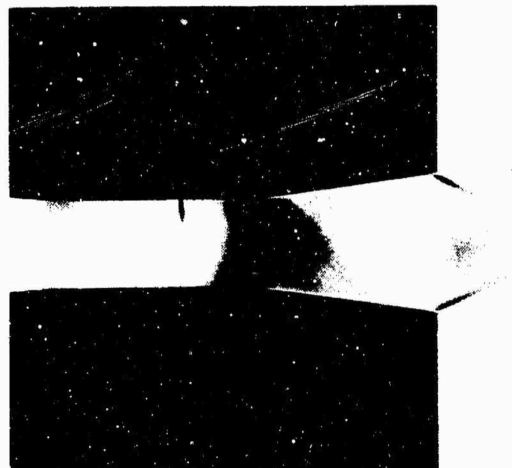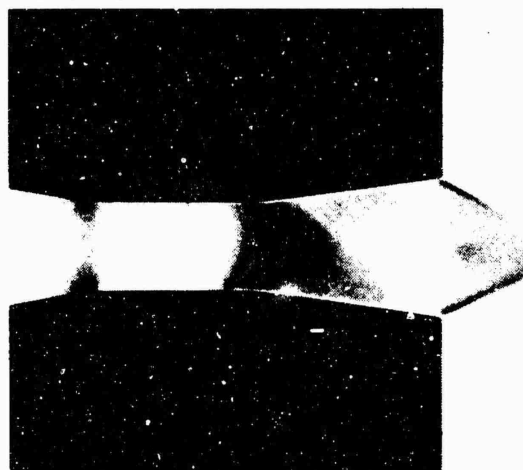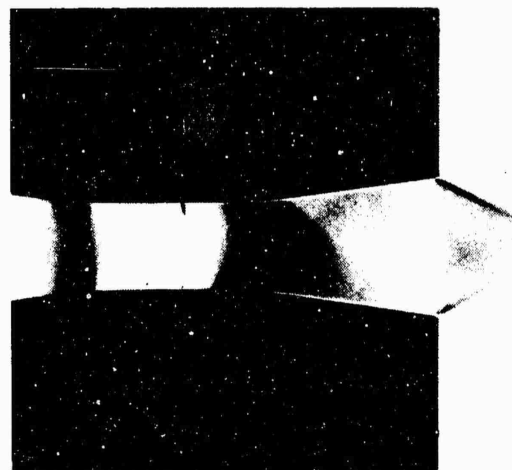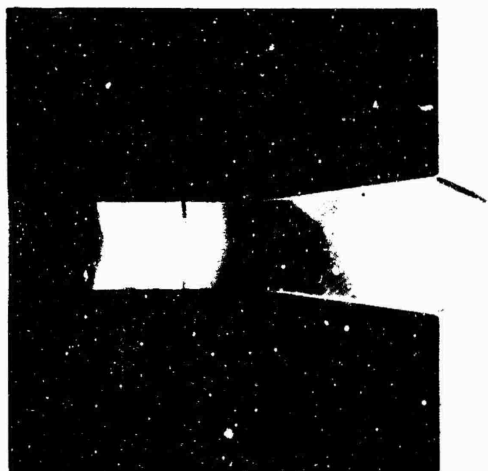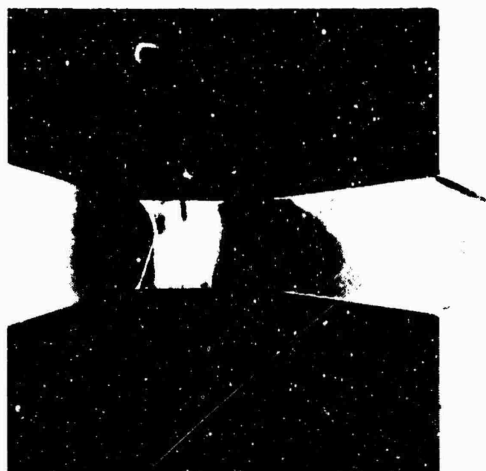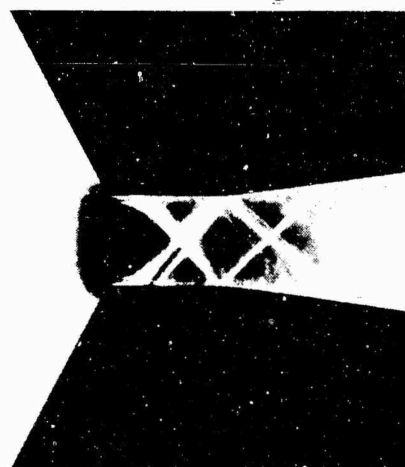(10)     30° ramp
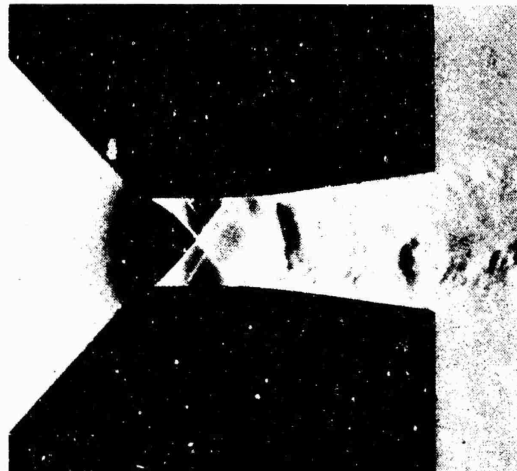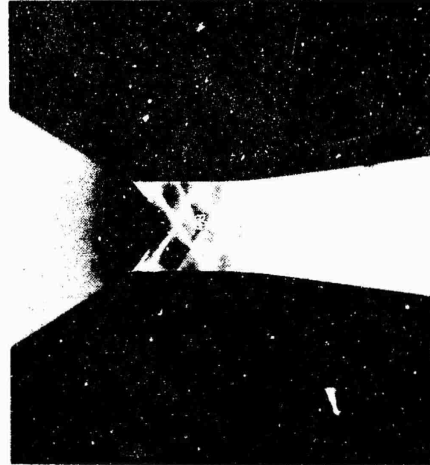
(11)     45° ramp
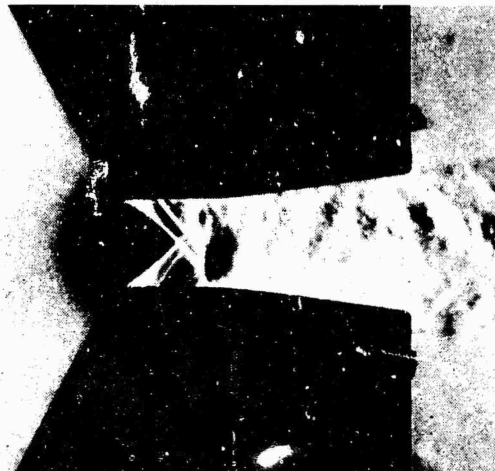
(12)     60° ramp

Schlieren Pictures of Various Nozzles at $P_a/P_o$ = 0.667

Fig A-2
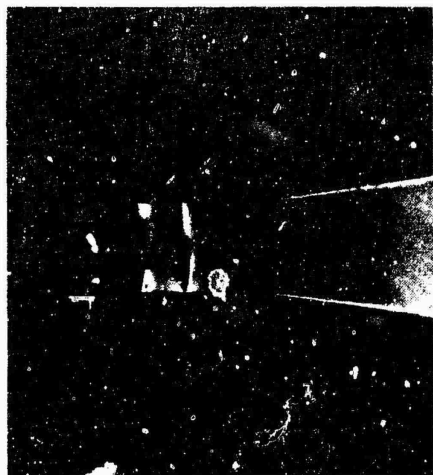
(1)  faired ellipse
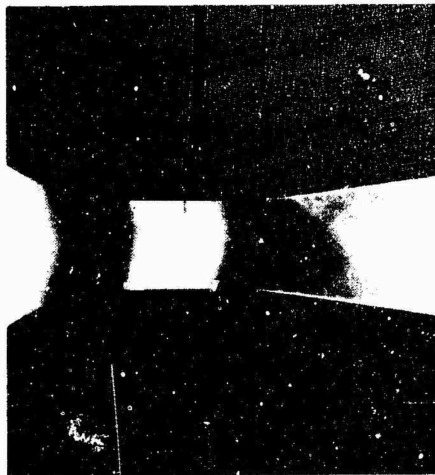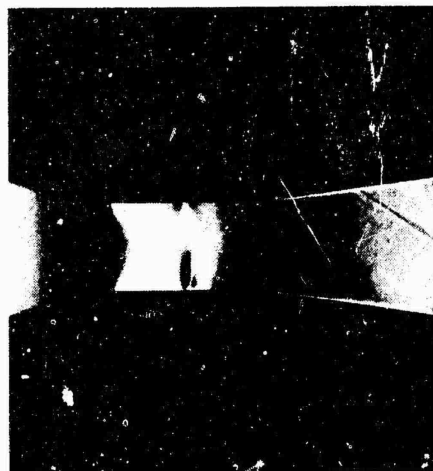
(2)  arc of radius 3h*

(3)  $y = e^X$ (short)
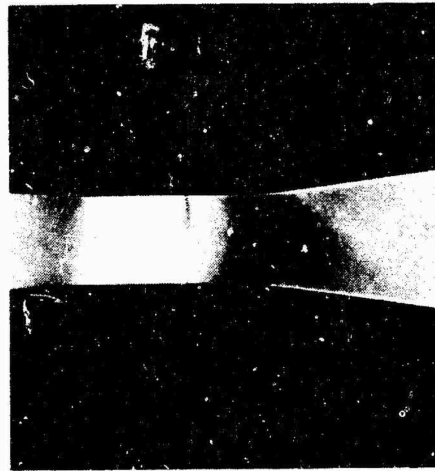
(4)      $M = kx$
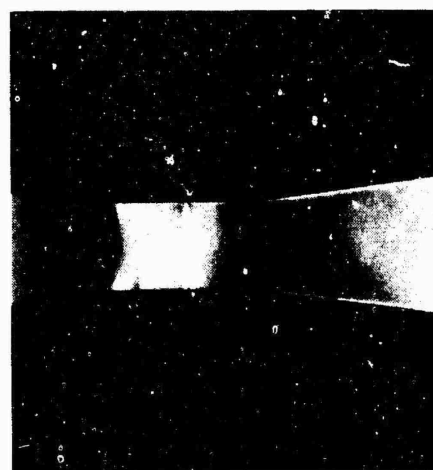
(5)  hyperbolic spiral

(6)    $y = e^X$ (long)

Schlieren Pictures of Various Nozzles at $P_a/P_o = 0\ 20$

Fig A-3
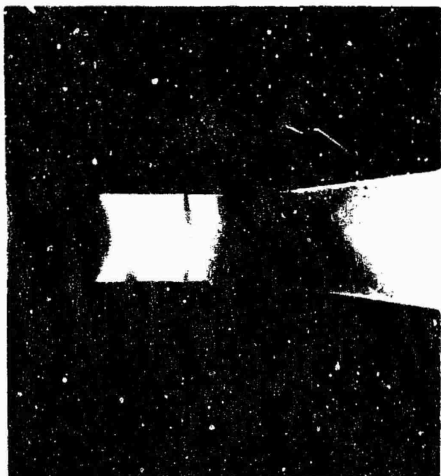
(7) arc of radius 5h*
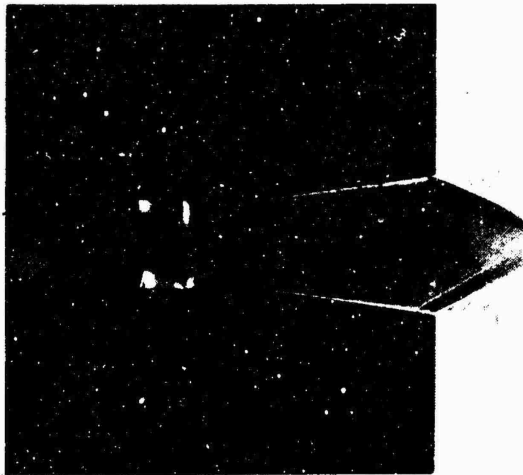
(8)  15° ramp

(9) arc of radius h*

(10)  30° ramp
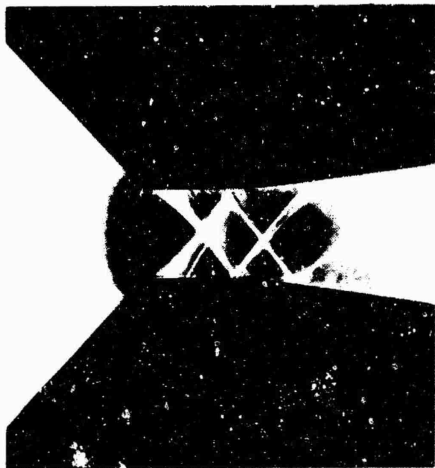
(11)  45° ramp
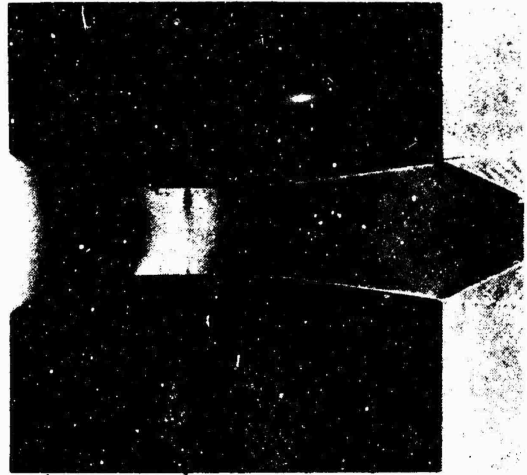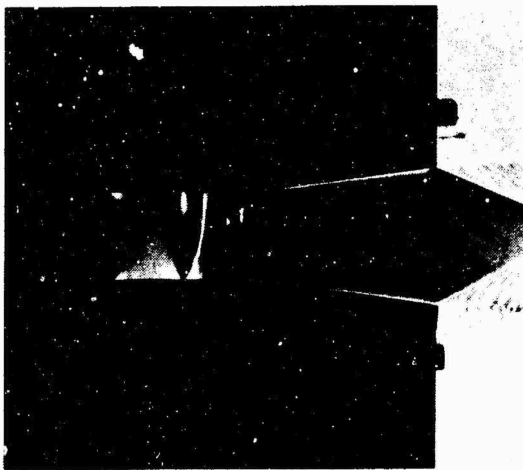
(12)  60° ramp

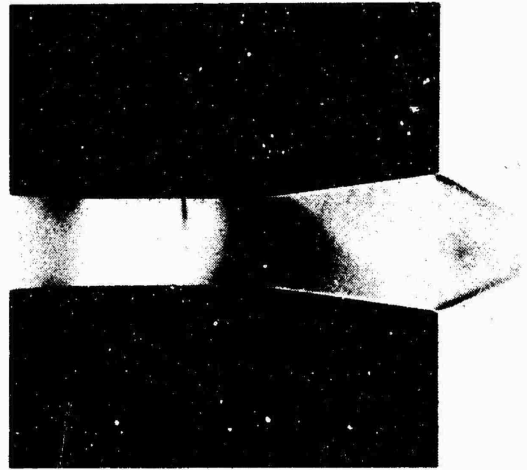Schlieren Pictures of Various Nozzles at Pa/Pc = 0.20

Fig A-4
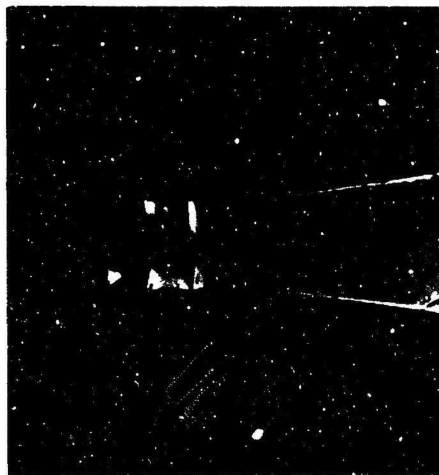
(1)  faired ellipse
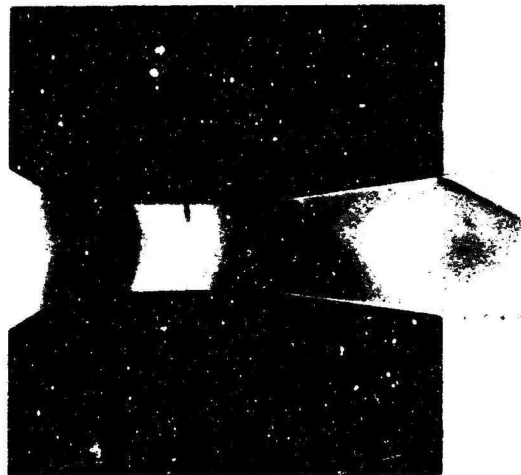
(2) arc of radius 3h*
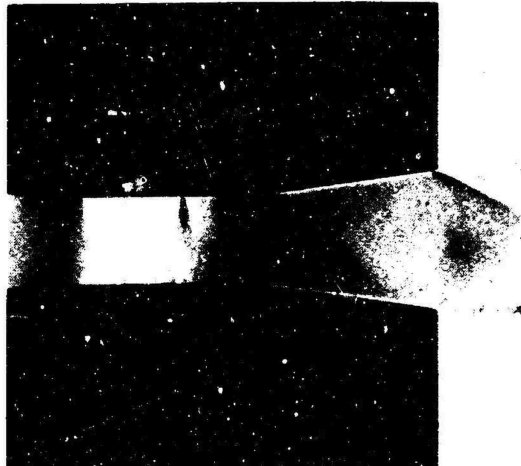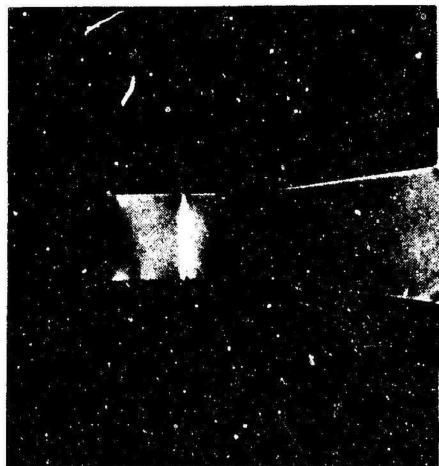
(3) $y = e^x$ (short)

(4)     M = kx

(5) hyperbolic spiral
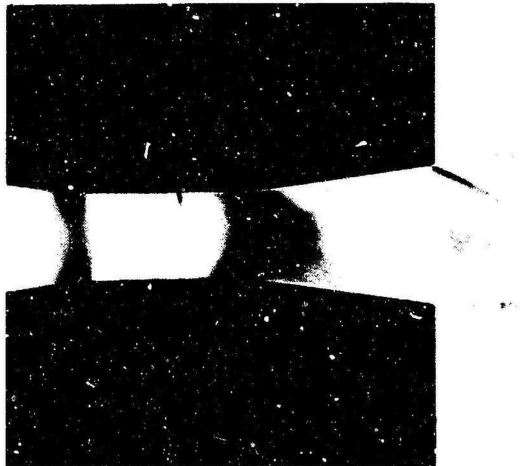
(6)    $y = e^x$ (long)

Schlieren Pictures of Various Nozzles at $P_a/P_o = 0.17$

Fig A-5
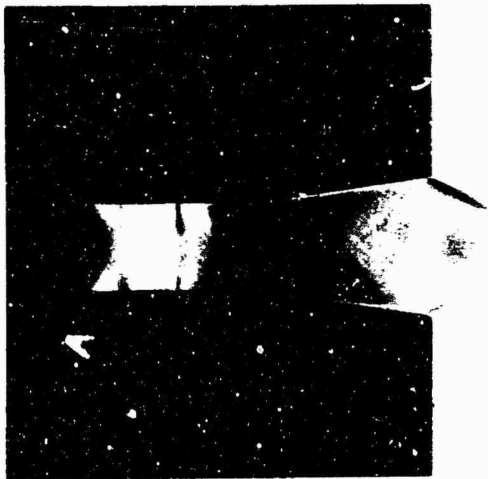
(7) arc of radius 5h*
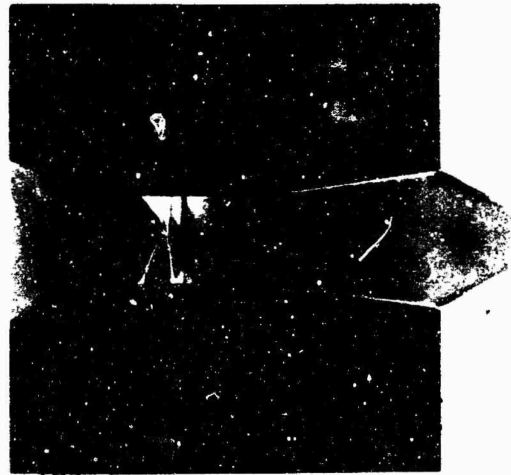
(8)        15° ramp
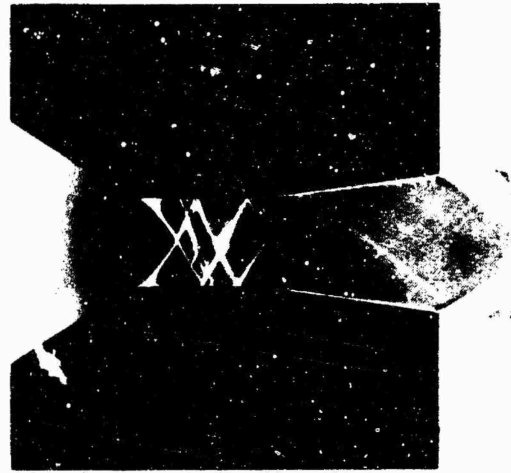
(9) arc of radius h*

(10)        30° ramp
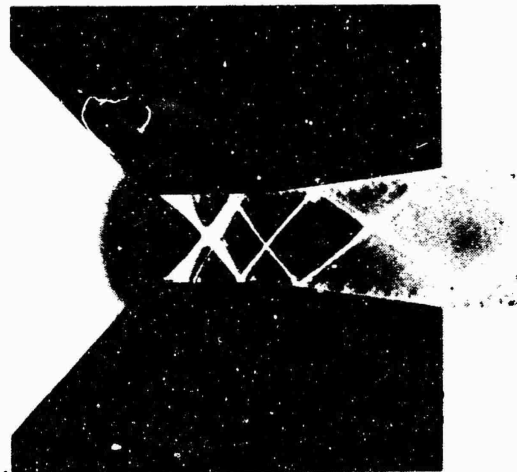
(11)        45° ramp
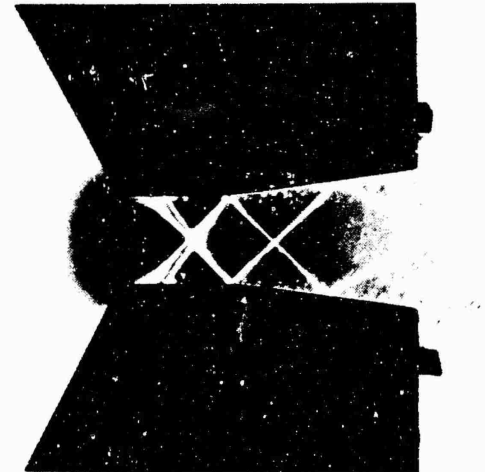
(12)        60° ramp

Schlieren Pictures of Various Nozzles at $P_a/P_o = 0.17$
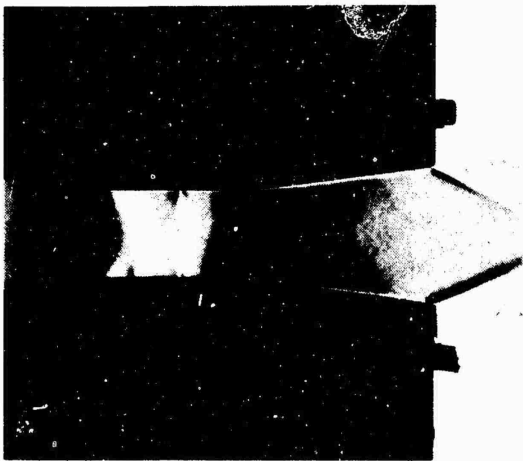
Fig A-6
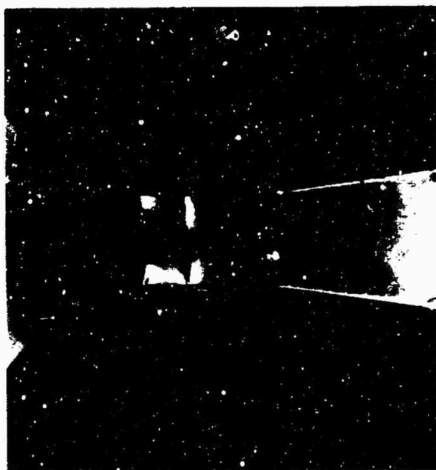
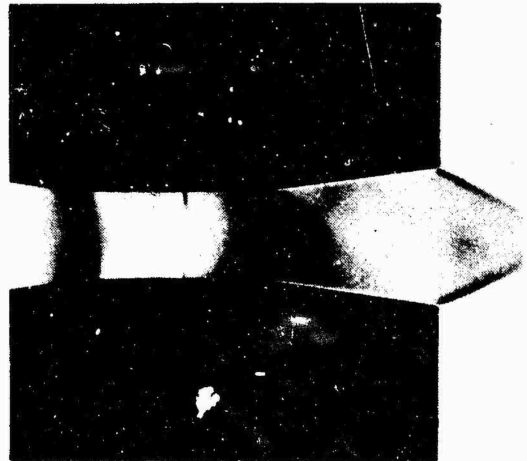(1)   faired ellipse
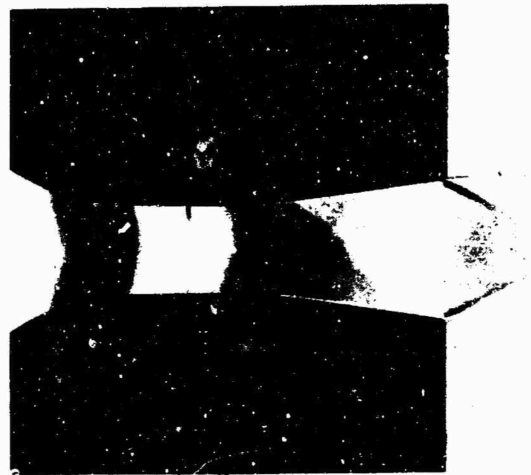
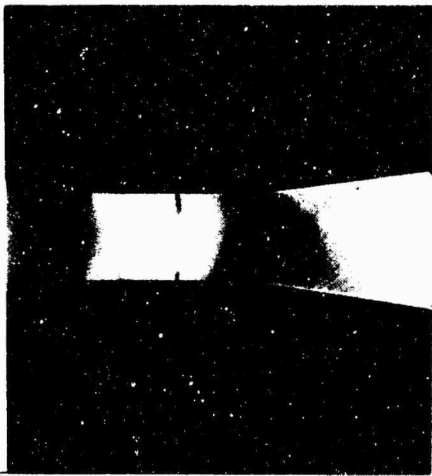(2)   arc of radius 3h*
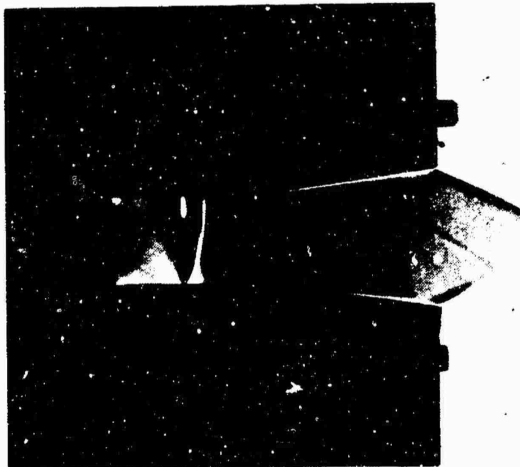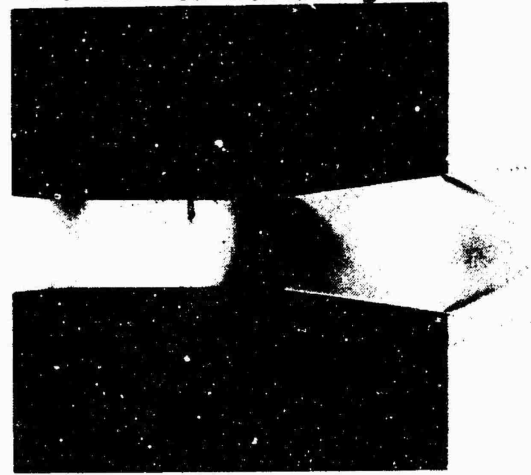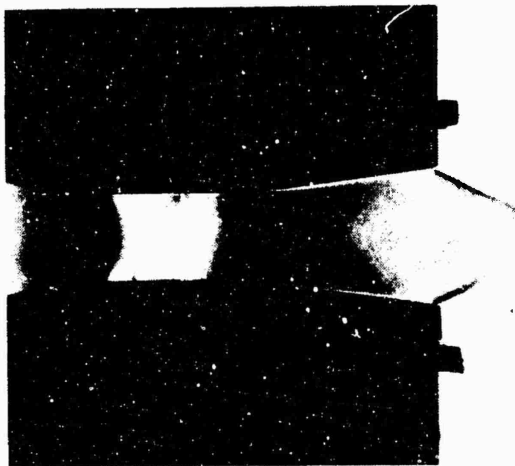
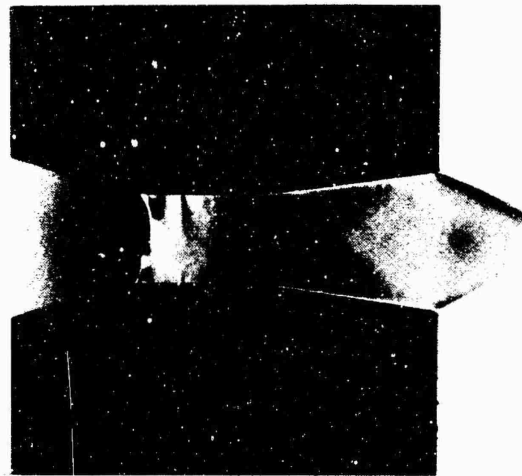(3)   $y = e^x$ (short)

(4)      M = kx

(5) hyperbolic spiral
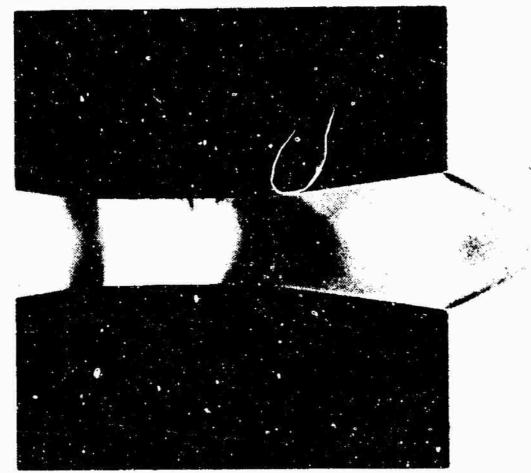
(6)   $y = e^x$ (long)

Schlieren Pictures of Various Nozzles at $P_a/P_o = 0.16$

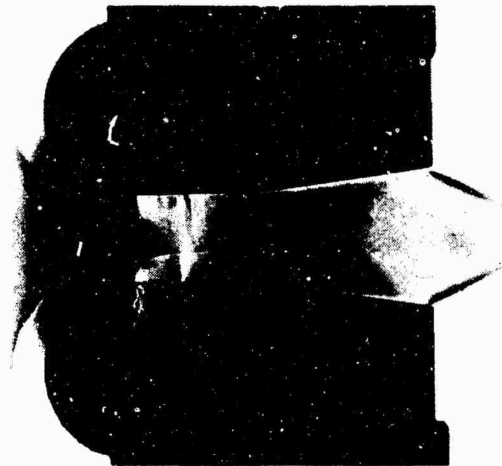Fig A-7
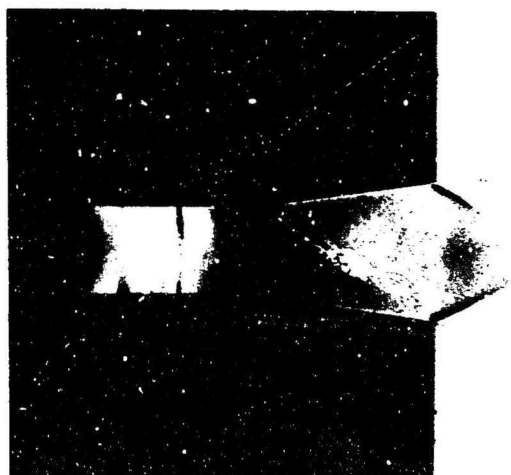
(7)  arc of radius 5h*

(8)       15° ramp

(9) arc of radius h*

(1C)      30° ramp
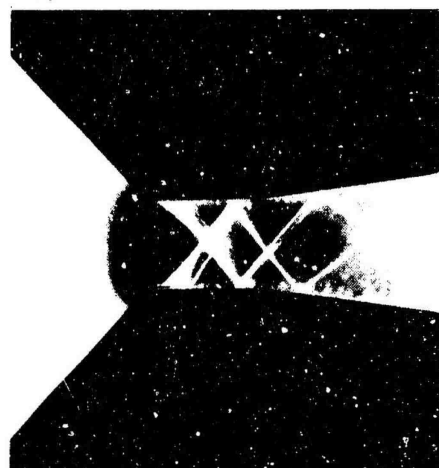
(11)      45° ramp

(12)      60° ramp

Schlieren Pictures of Various Nozzles at $P_a/P_o = 0.16$

Fig A-8

(1) faired ellipse


(2) arc of radius 3h*


(3) $y = e^x$ (short)


(4) $M = kx$


(5) hyperbolic spiral


(6) $y = e^x$ (long)

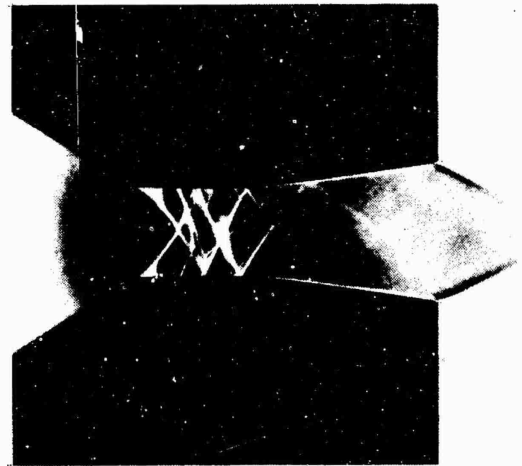Schlieren Pictures of Various Nozzles at $P_a/P_o = 0.156$

Fig A-9

(7) arc of radius 5h*


(8)     15º ramp


(9) arc of radius h*


(10)    30º ramp


(11)    45º ramp


(12)    60º ramp

Schlieren Pictures of Various Nozzles at $P_a/P_o$ = 0.156

Fig A-10

(1)  faired ellipse

(2)  arc of radius 3h*

(3)  y = e^x (short)

(4)        M = kx

(5) hyperbolic spiral

(6)    y = e^x (long)

Schlieren Pictures of Various Nozzles at $P_a/P_o$ = 0.15

Fig A-11

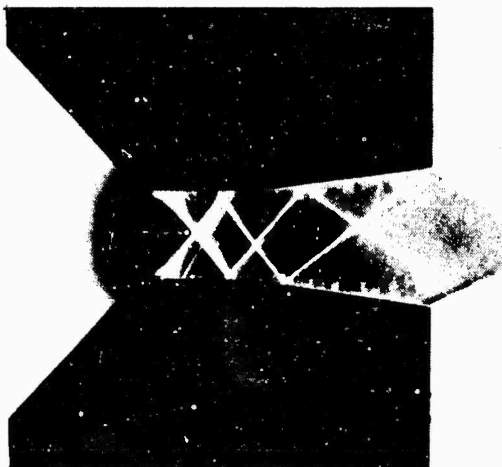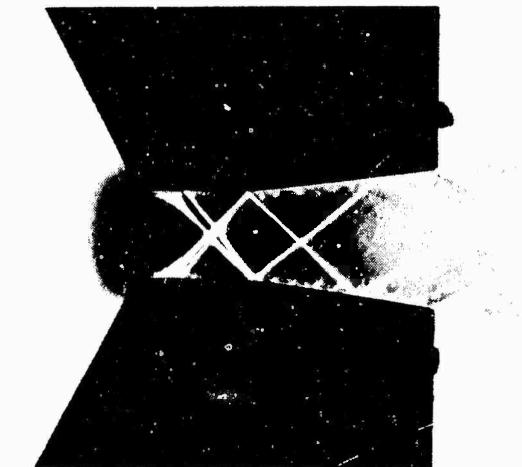(7) arc of radius 5h*                  (8)          15° ramp

(9) arc of radius h*                   (10)         30° ramp
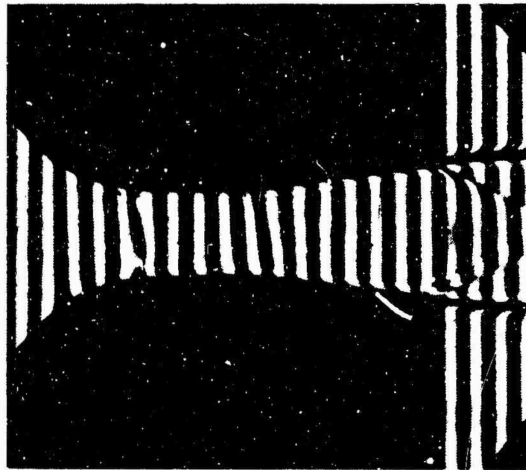
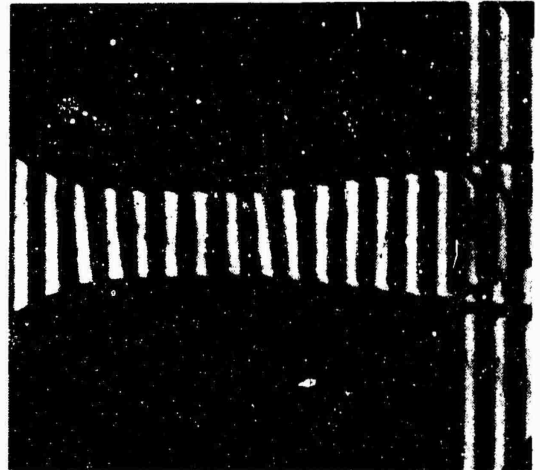(11)         45° ramp                  (12)         60° ramp

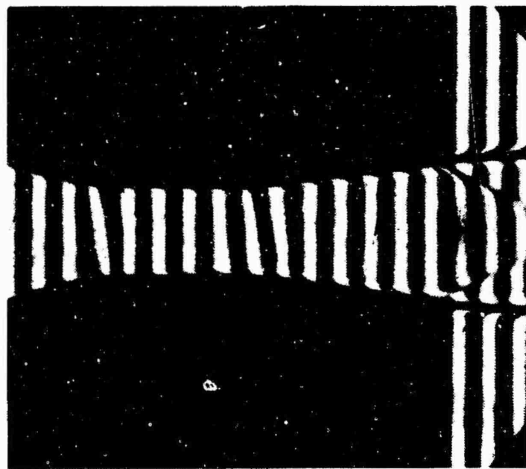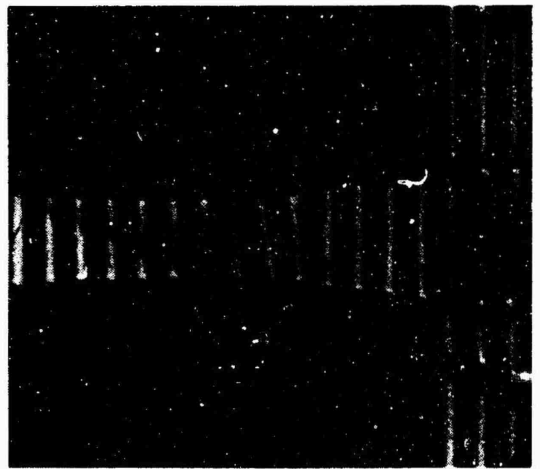Schlieren Pictures of Various Nozzles at $P_a/P_o = 0.15$

Fig A-12

(1)   faired ellipse
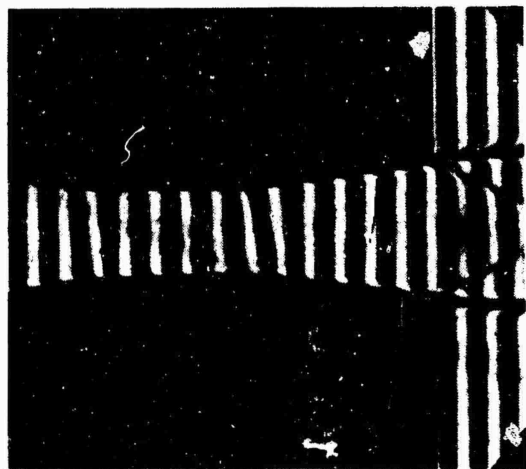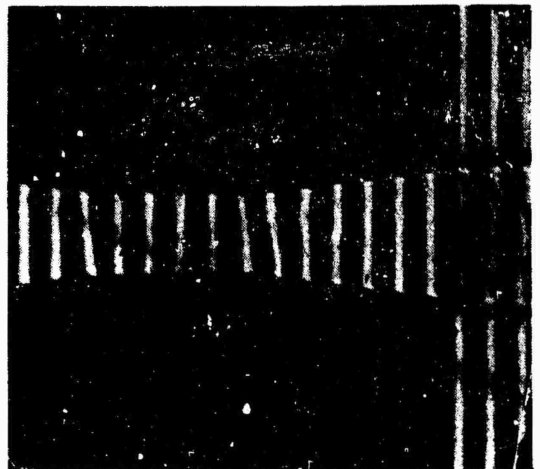
(2)  arc of radius 3h*

(3)   $y = e^x$ (short)

(4)      M = kx

(5)  hyperbolic spiral

(6)   $y = e^x$ (long)

Moire' Patterns for Various Inlet Contours at $P_a/P_o = 0.156$
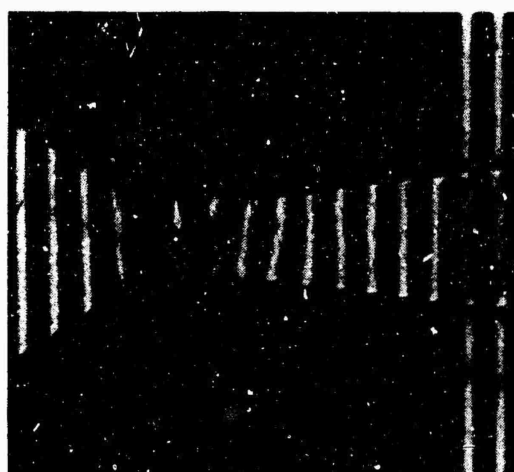
Fig A-13

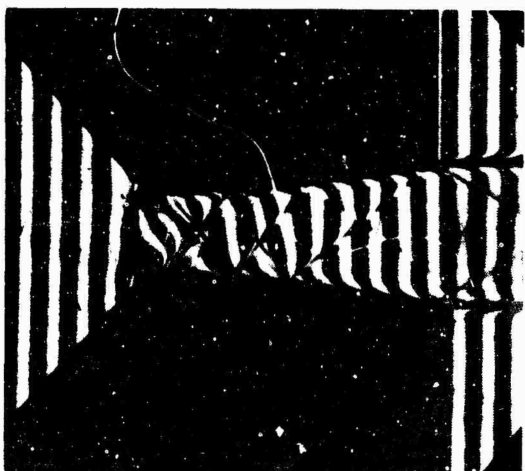(7) arc of radius 5h*       (8)      15° ramp

(9) arc of radius h*      (10)      30° ramp

(11)      45° ramp      (12)      60° ramp

Moire' Patterns for Various Inlet Contours at $P_a/P_o = 0.156$

Fig A-14

Appendix B

Graphs of Experimental Data

Fig B-1

Fig B-2

Variation of Total Pressure
Across Nozzle Exit

Fig B-3

Fig B-4

Variation of Total Pressure
Across Nozzle Exit

Fig B-5

Fig B-6

60° ramp

Effect of Averaging
Total Pressure

position 1
position 2
position 3
average

faired ellipse

Effect of Averaging
Total Pressure

position 1
position 2
position 3
average

Fig B-7

Variation of Static Pressure
Along Nozzle Axis

Variation of Static Pressure
Along Nozzle Axis

Fig B-8

Variation of Static Pressure
Along Nozzle Axis

Variation of Static Pressure
Along Nozzle Axis

Fig B-9

Fig B-10

Variation of Static Pressure
Along Nozzle Axis

Variation of Static Pressure
Along Nozzle Axis

Fig B-11

Variation of Static Pressure
Along Nozzle Axis

Variation of Static Pressure
Along Nozzle Axis

Fig B-12

Variation of Static Pressure
Along Nozzle Axis

Variation of Static Pressure
Along Nozzle Axis

Fig B-13

Fig B-14

Variation of Temperature Gradient With Distance From Throat Entrance for Various Nozzle Contours

Variation of Temperature Gradient With Distance From Throat Entrance for Various Nozzle Contours
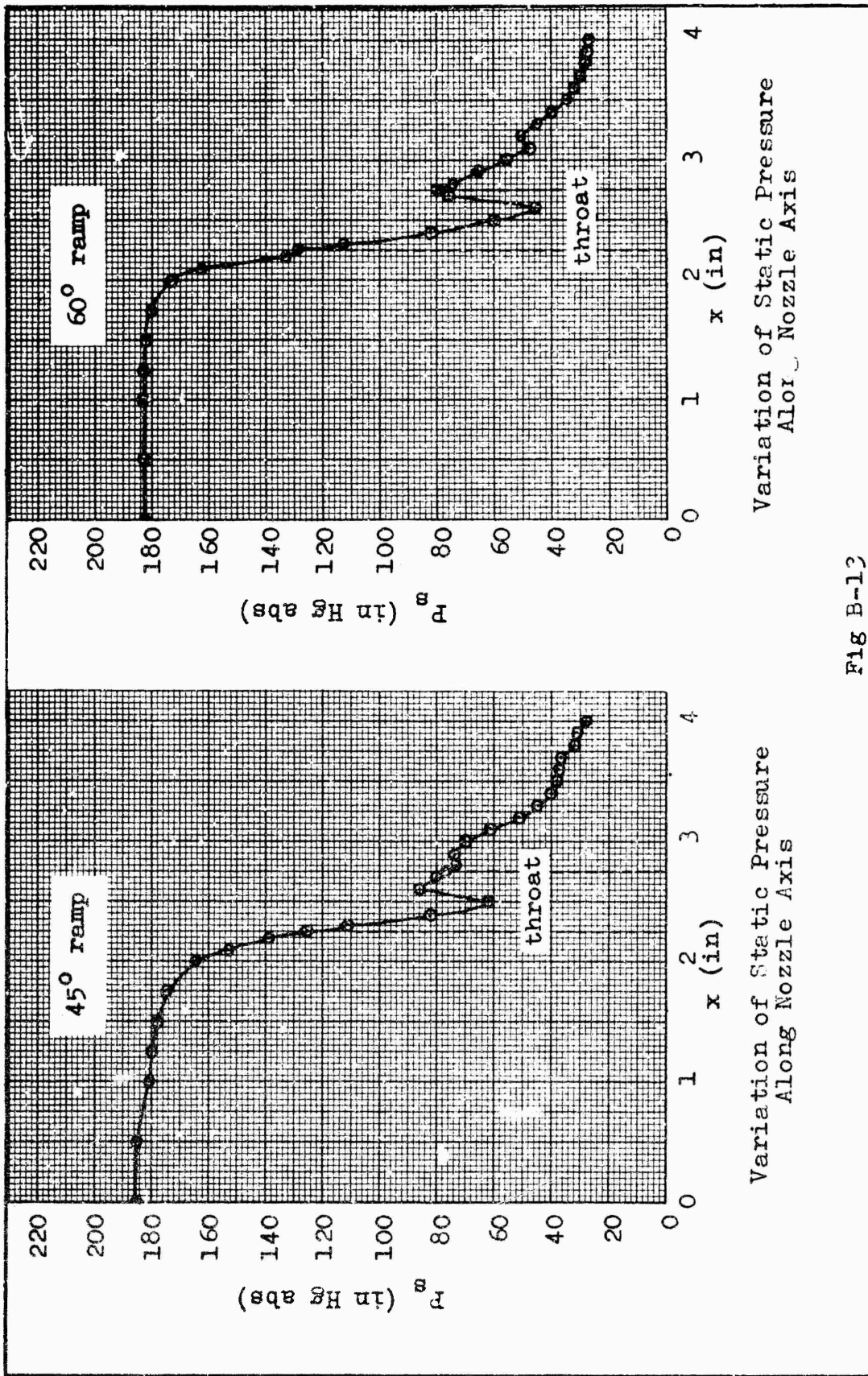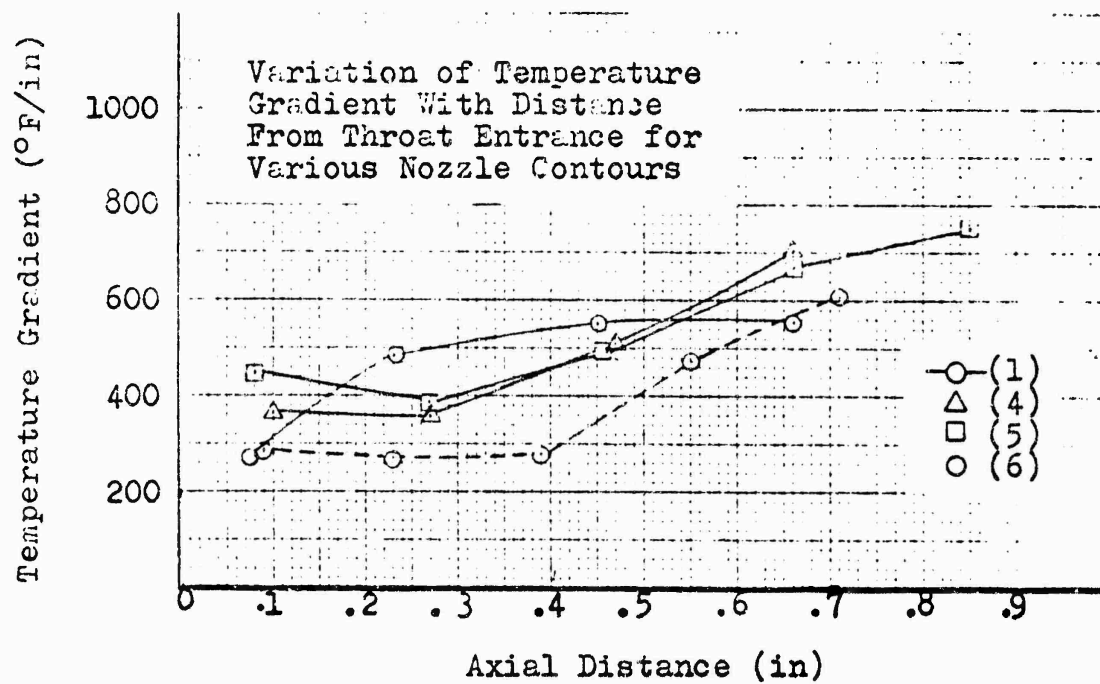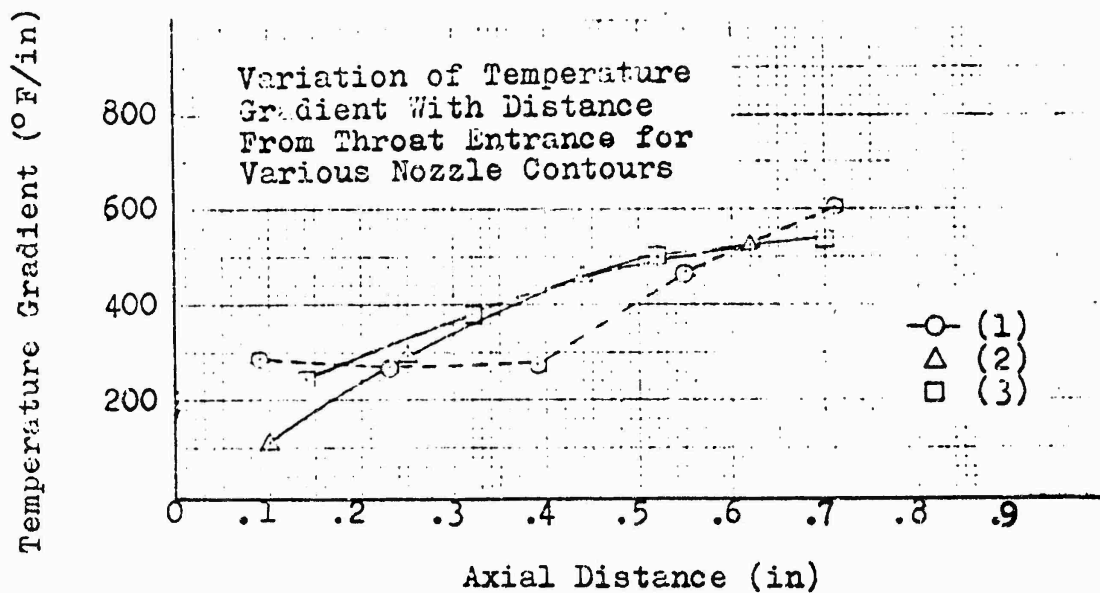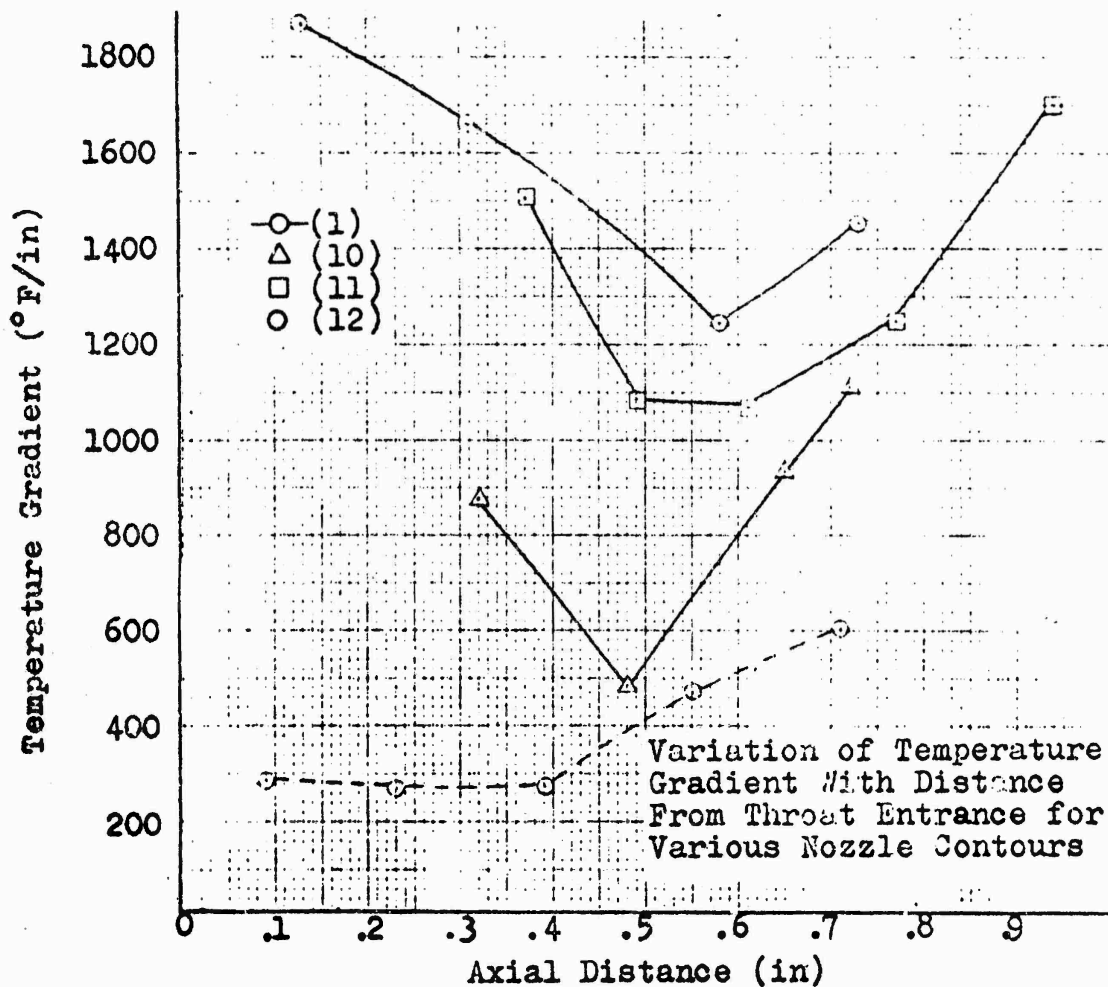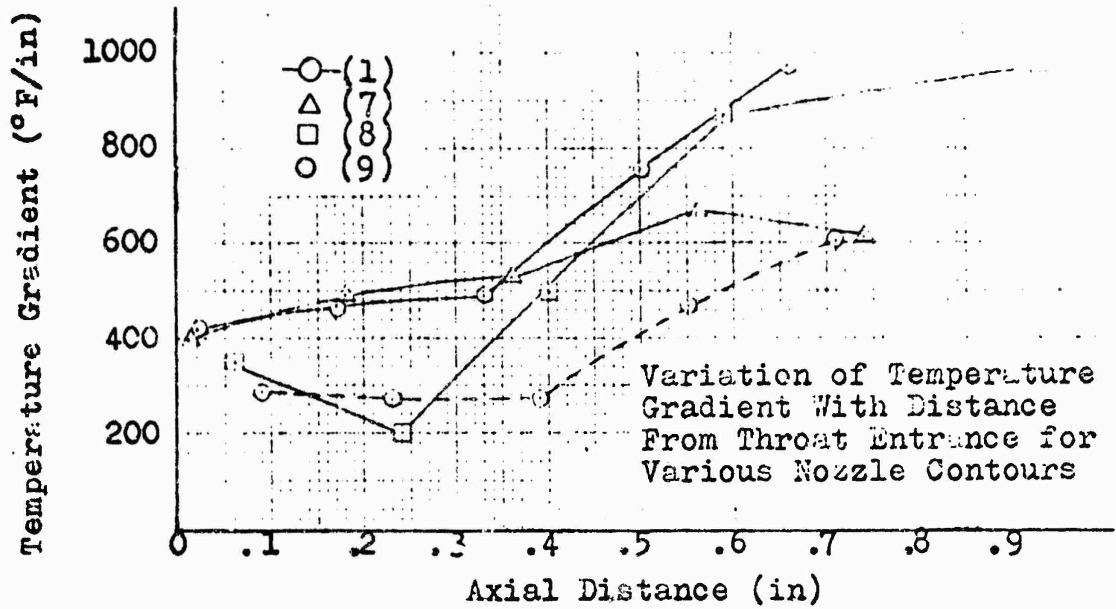
Fig B-15

Appendix C

Detail Drawings

TWO DIMENSIONAL NOZZLE
1"=1" PROJECT NO. GAM/ME/6911
LT GERALD M. MULENBURG
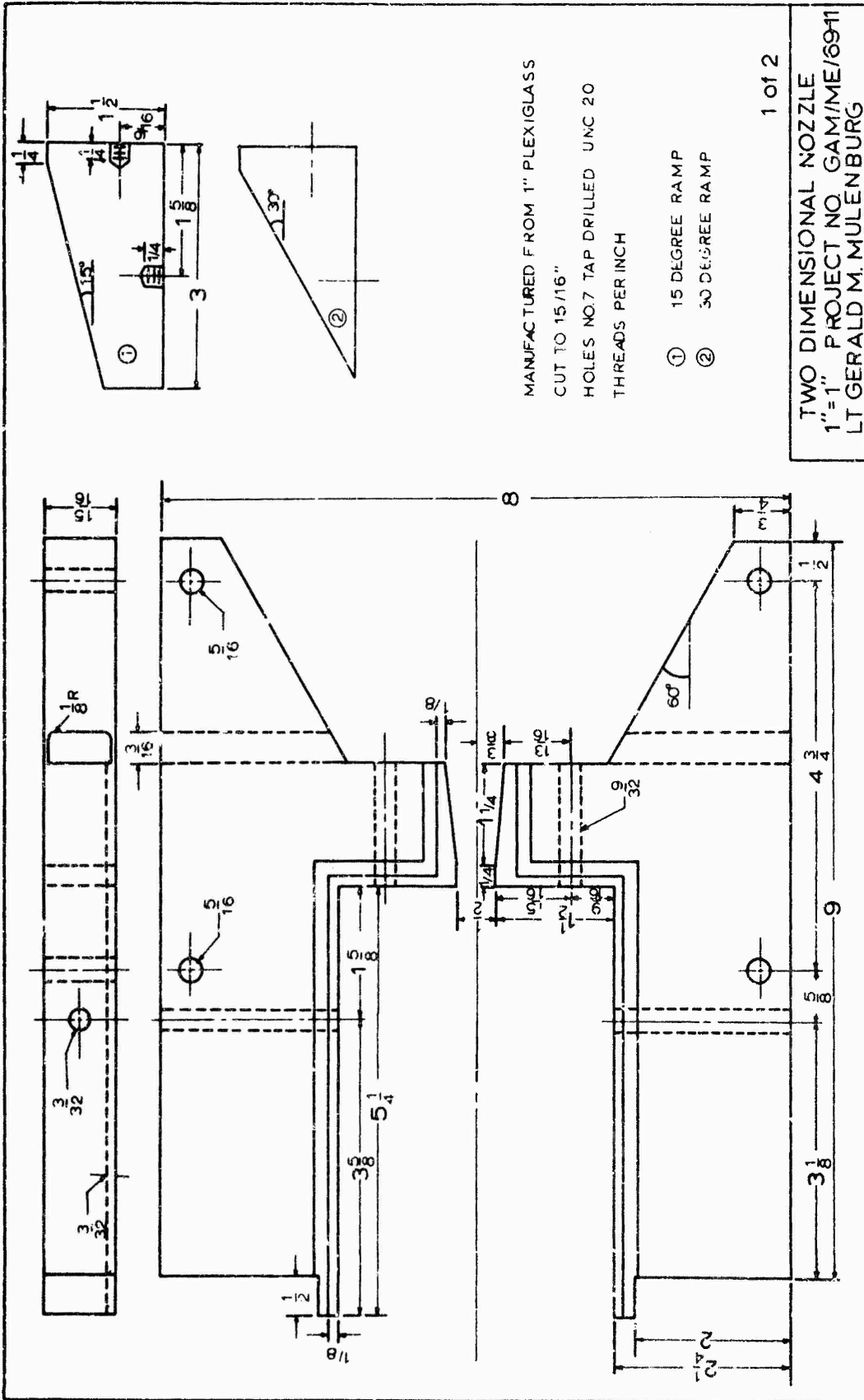
1 of 2

MANUFACTURED FROM 1" PLEXIGLASS

CUT TO 15/16"

HOLES NO.7 TAP DRILLED UNC 20

THREADS PER INCH

① 15 DEGREE RAMP

② 30 DEGREE RAMP

Fig C-1

INLET BLOCKS
1"=1" PROJECT NO.GAM/ME/69-11
LT GERALD M. MULENBURG

2 of 2

3 HYPERBOLIC SPIRAL
4 $Y = e^x$
5 $Y = e^x$
6 45° RAMP
7 60° RAMP

8 $M = KX$ (K=0.182)
9 ARC OF RADIUS h°
10 FAIRED ELLIPSE
11 ARC OF RADIUS 5h°
12 ARC OF RADIUS 3h°
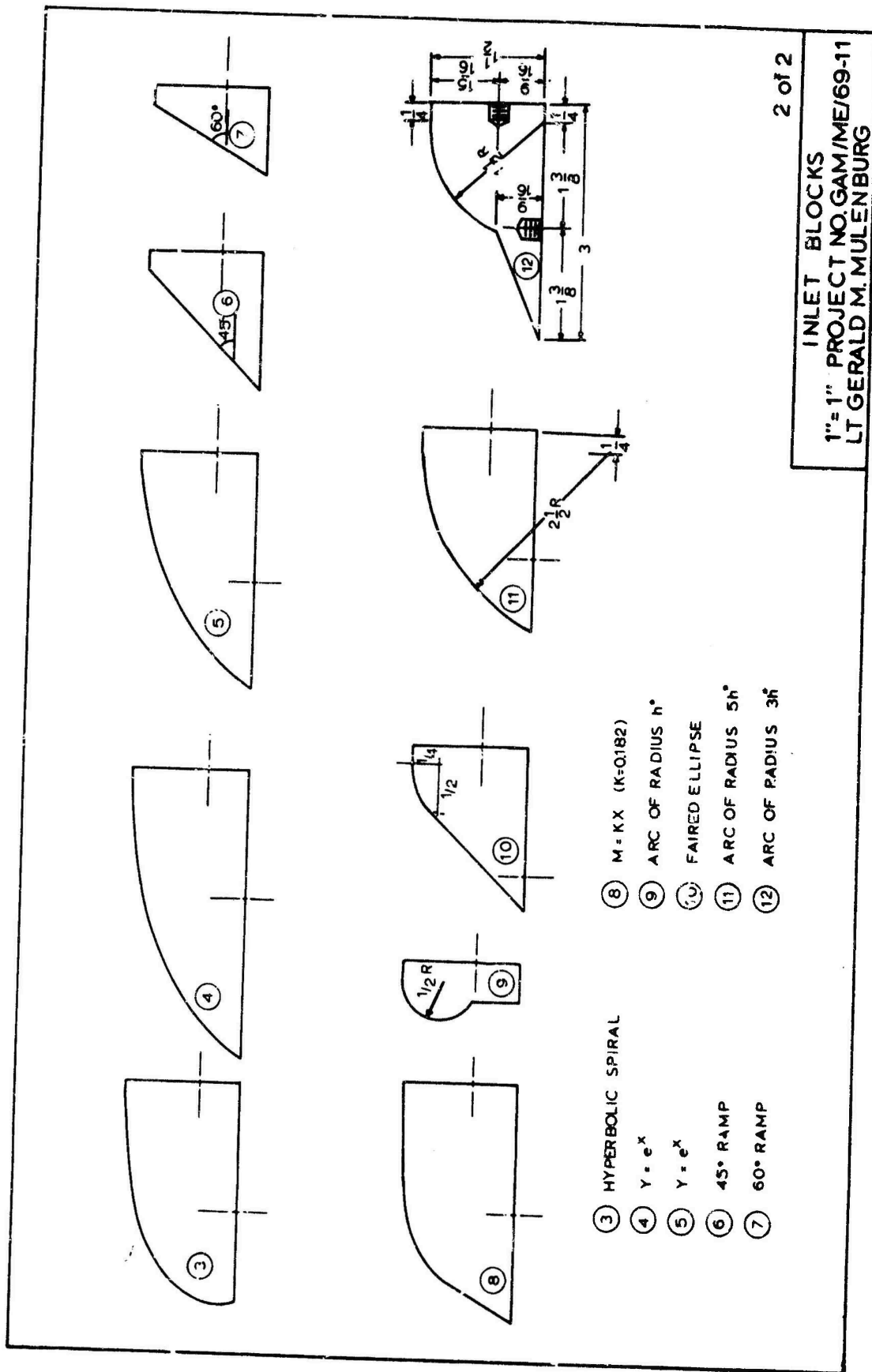
Fig C-2

## Vita

Gerald Martin Mulenburg was born ███████████████

████████████████████ ████████████████████
██████████ After attending ███████████████
██████████ he enlisted in the Air Force in January
1956. He attended Oklahoma State University through the
Airman Education and Commissioning Program and in January
1967 recieved a Bachelor of Science degree in Aero-Mechan-
ical Engineering. Completing Officer Training School as a
Distinguished Graduate in April 1967, he was commissioned
a 2nd Lieutenant in the Air Force Reserve and assigned to
the Air Force Institute of Technology for Graduate study in
Aerospace-Mechanical Engineering.

Permanent address: ████████████████
████████████ ███████████

This thesis was typed by ███████████████████

## DOCUMENT CONTROL DATA - R & D

*(Security Classification of title, body of abstract and indexing annotation must be entered when the overall report is classified)*

| 1. ORIGINATING ACTIVITY (Corporate author) | 2a. REPORT SECURITY CLASSIFICATION |
|---|---|
| Air Force Institute of Technology (AFIT-SE) Wright-Patterson Air Force Base, Ohio 45433 | Unclassified |
| | 2b. GROUP |

3. REPORT TITLE

An Experimental Study of the Effect of Inlet Geometry on Flow and Performance of a Supersonic Nozzle

4. DESCRIPTIVE NOTES (Type of report and inclusive dates)

AFIT Thesis

5. AUTHOR(S) (First name, middle initial, last name)

Gerald M. Mulenburg
First Lieutenant   USAF

| 6. REPORT DATE | 7a. TOTAL NO. OF PAGES | 7b. NO. OF REFS |
|---|---|---|
| 28 February 1969 | 56 | 6 |

| 8a. CONTRACT OR GRANT NO. | 9a. ORIGINATOR'S REPORT NUMBER(S) |
|---|---|
| b. PROJECT NO.  N/A | GAM/ME/69-11 |
| c. | 9b. OTHER REPORT NO(S) (Any other numbers that may be assigned this report) |
| d. | |

10. DISTRIBUTION STATEMENT This document is subject to special export controls and each transmittal to foreign governments or foreign nationals may be made only with prior approval of the Dean of Engineering, Air Force Institute of Technology (AFIT-SE), Wright-Patterson Air Force Base, Ohio 45433

| 11. SUPPLEMENTARY NOTES | 12. SPONSORING MILITARY ACTIVITY |
|---|---|
| | |

13. ABSTRACT This study is an experimental evaluation of the performance of 12 two-dimensional, converging-diverging, cold flow, supersonic nozzles, each with the same throat and divergent section. The relative efficiency of each nozzle was evaluated by a comparison of total pressure measurements taken in the exit plane, schlieren photographs of the flow, and heat transfer characteristics using moire' patterns. The nozzle with the highest efficiency had an inlet which was an ellipse faired to a $45^\circ$ ramp. Its performance was closely followed by that of a nozzle with a circular arc inlet having a radius of three times the throat height. The three nozzles with the lowest efficiencies were those with $30^\circ$, $45^\circ$, and $60^\circ$ linear ramp inlets, respectively. The results of this study indicate that, in nozzle design, a region of immense importance is the curvature just prior to the throat and how this curvature is joined to the throat section.

DD FORM 1473
I NOV 65

| 14. KEY WORDS | LINK A | | LINK B | | LINK C | |
|---|---|---|---|---|---|---|
| | ROLE | WT | ROLE | WT | ROLE | WT |
| Nozzle Inlet Design | | | | | | |
| Nozzle Geometry | | | | | | |
| Nozzle Performance | | | | | | |
| Inlet contour | | | | | | |